RADC-TR-88-96
Interim Report
July 1988

RECONFIGURABLE ANTENNAS

University of Illinois

Y. T. Lo, S. L. Chuang, P. Aoyagi,
J. Brenneman and M. Davidovitz

APPROVED FOR PUBLIC RELEASE; DISTRIBUTION UNLIMITED.

ROME AIR DEVELOPMENT CENTER
Air Force Systems Command
Griffiss Air Force Base, NY 13441-5700

This report has been reviewed by the RADC Public Affairs Division (PA) and is releasable to the National Technical Information Service (NTIS). At NTIS it will be releasable to the general public, including foreign nations.

RADC-TR-88-96 has been reviewed and is approved for publication.

APPROVED: Charles J. Drane

CHARLES J. DRANE
Project Engineer

APPROVED: John K. Schindler

JOHN K. SCHINDLER
Acting Director of Electromagnetics

FOR THE COMMANDER: John A. Ritz

JOHN A. RITZ
Directorate of Plans & Programs

If your address has changed or if you wish to be removed from the RADC mailing list, or if the addressee is no longer employed by your organization, please notify RADC (EEAA) Hanscom AFB MA 01731-5000. This will assist us in maintaining a current mailing list.

Do not return copies of this report unless contractual obligations or notice on a specific document requires that it be returned.

UNCLASSIFIED
SECURITY CLASSIFICATION OF THIS PAGE

REPORT DOCUMENTATION PAGE

Form Approved OMB No. 0704-0188

1a. REPORT SECURITY CLASSIFICATION UNCLASSIFIED	1b. RESTRICTIVE MARKINGS N/A
2a. SECURITY CLASSIFICATION AUTHORITY N/A	3. DISTRIBUTION/AVAILABILITY OF REPORT Approved for public release; distribution unlimited.
2b. DECLASSIFICATION/DOWNGRADING SCHEDULE N/A	
4. PERFORMING ORGANIZATION REPORT NUMBER(S) EM 86-10; UILU-ENG-86-2558	5. MONITORING ORGANIZATION REPORT NUMBER(S) RADC-TR-88-96
6a. NAME OF PERFORMING ORGANIZATION University of Illinois 6b. OFFICE SYMBOL (If applicable)	7a. NAME OF MONITORING ORGANIZATION Rome Air Development Center (EEAA)
6c. ADDRESS (City, State, and ZIP Code) Department of Electrical & Computer Engineering 1406 W. Green Street Urbana IL 61801-2991	7b. ADDRESS (City, State, and ZIP Code) Hanscom AFB MA 01731-5000
8a. NAME OF FUNDING/SPONSORING ORGANIZATION Rome Air Development Center 8b. OFFICE SYMBOL (If applicable) EEAA	9. PROCUREMENT INSTRUMENT IDENTIFICATION NUMBER F19628-85-K-0052
8c. ADDRESS (City, State, and ZIP Code) Hanscom AFB MA 01731-5000	10. SOURCE OF FUNDING NUMBERS PROGRAM ELEMENT NO. 61102F; PROJECT NO. 2305; TASK NO. J3; WORK UNIT ACCESSION NO. 48

11. TITLE (Include Security Classification)
RECONFIGURABLE ANTENNAS

12. PERSONAL AUTHOR(S)
Y. T. Lo, S. L. Chuang, P. Aoyagi, J. Brenneman and M. Davidovitz

13a. TYPE OF REPORT	13b. TIME COVERED	14. DATE OF REPORT (Year, Month, Day)	15. PAGE COUNT
Interim	FROM Sep 85 TO Sep 86	July 1988	76

16. SUPPLEMENTARY NOTATION
N/A

17. COSATI CODES			18. SUBJECT TERMS (Continue on reverse if necessary and identify by block number)
FIELD	GROUP	SUB-GROUP	
17	02		Microstrip Antennas, Coplanar Waveguide Feed for Integrated Active Antennas, Microstrip Antennas, Electromagnetic Feed for Microstrip Antennas
17	03		

19. ABSTRACT (Continue on reverse if necessary and identify by block number)

Engineering investigations were conducted in several areas related to the analysis and design of an integrated phased array utilizing microstrip antenna elements. Two types of electromagnetically coupled feed structures for microstrip antenna elements were examined in greater detail. An amplifier design, compatible with the electromagnetic feed, was synthesized. An integrated "active" array element with a coplanar waveguide feed was constructed and tested. Preliminary testing of the "active" element has shown that it has very good performance characteristics. The active amplifier adds 13 dB of gain to the antenna element. A two-element passive array utilizing electromagnetically coupled feeds was also designed, constructed and tested. Finally, a rigorous full-wave analysis was made for a circular patch antenna electromagnetically fed with a microstrip line directly underneath the patch. The results show that a properly designed system can have efficient coupling and excitation for the antenna.

20. DISTRIBUTION/AVAILABILITY OF ABSTRACT	21. ABSTRACT SECURITY CLASSIFICATION
☐ UNCLASSIFIED/UNLIMITED ☒ SAME AS RPT ☐ DTIC USERS	UNCLASSIFIED
22a. NAME OF RESPONSIBLE INDIVIDUAL Charles J. Drane	22b. TELEPHONE (Include Area Code) (617) 377-2051 22c. OFFICE SYMBOL RADC (EEAA)

DD Form 1473, JUN 86 *Previous editions are obsolete.*

SECURITY CLASSIFICATION OF THIS PAGE
UNCLASSIFIED

TABLE OF CONTENTS

CHAPTER I.

MICROSTRIP ANTENNA STRUCTURE

Of the various types of electromagnetically coupled feed structures, the coplanar ones, commonly referred to in the literature as slot line and coplanar waveguide, are of special interest because of the ease with which active devices with a planar architecture are integrated with the antenna elements. Engineering efforts made during the last period were therefore concentrated on analysing and understanding the coplanar structures.

Our preliminary experiments showed that it was possible to efficiently excite the microstrip antenna with the coplanar waveguide feed. Subsequent analysis and experiments were performed to understand the excitation mechanism with the goal of developing an analytic model that can predict the performance of the antenna.

To simplify the analysis, several assumptions are made. The dimensions of the antenna are such that the cavity model for the antenna can be invoked. The slots in the coplanar waveguide are narrow compared to the width of the center conductor. This results in a low impedance transmission line with the electric fields concentrated within the slots. The coplanar waveguide can be analysed as two parallel coupled slot lines on which an odd mode has been excited. Huygens' principle can be applied to the slot and one obtains an equivalent magnetic current source, equal in magnitude but opposite in phase, for each slot. If an even mode has also been excited on the coplanar waveguide the current sources will not be equal in magnitude.

A basic insight into the coupling mechanism for a coplanar feed is given by the energy relation for electromagnetic fields stated below.

$$P_S = \oint_S (\hat{H}\cdot\hat{K} + \hat{E}\cdot\hat{J})\cdot d\hat{S} = \frac{\partial}{\partial t}\int_V (\tfrac{1}{2}\varepsilon_0 E^2 + \tfrac{1}{2}\mu_0 H^2)\, dV + \int_V \sigma E^2 dV + \oint_S \hat{E}\times\hat{H}\cdot d\hat{S}$$

P_S = Power Supplied to Antenna

$\int_V (\tfrac{1}{2}\varepsilon_0 E^2 + \tfrac{1}{2}\mu_0 H^2)\, dV$ = Total Stored Energy

$\int_V \sigma E^2 dV$ = Total Dissipated Power

$\oint_S \hat{E}\times\hat{H}\cdot d\hat{S}$ = Total Radiated Power

There must be a source component in parallel with the field component that is to be excited. The larger the mean value of the scalar product of the source and field components is over a closed surface, the greater the power supplied to the region under consideration. For example, by feeding the patch antenna by a coplanar waveguide as indicated in Fig. 1, it is possible to excite the (0,1) mode. In the (0,1) mode the magnetic field, H, is oriented in the x direction, and it goes to zero on the magnetic walls at y=0 and y=b. It has maximum magnitude at y=b/2. There is no variation in the x direction inside the cavity for the (0,1) mode. The electric fields are in the z direction and are zero along the line y=b/2 inside the cavity. At the end of the coplanar waveguide feed, the equivalent magnetic current source, K, is oriented in the x direction. This source component is in parallel with the magnetic field, H, of the (0,1) mode and should, therefore, excite that cavity mode. The y directed components of the source, K, should have little effect on the dominant

(0,1) mode but may excite other modes. Maximum excitation should occur when the feed is terminated at the center of the patch where the magnetic field is maximum. As the feed is terminated closer to the edges of the patch, the excitation should go to zero as the magnetic field goes to zero. Note that excitation of the cavity occurs along the line y=b/2 even though the electric field is zero along that line. Table 1 lists antenna input impedance versus feed location. These impedance values have been measured at a plane extended several wavelengths from the edge of the patch antenna. At this point, to build a good qualitative picture of input impedance versus feed location, the magnitude of the input impedance is the parameter of primary interest and the phase shift due to the extended measurement plane is of secondary importance. (Time domain reflectometry was used to insure a near perfect transition from a coaxial transmission line to the coplanar waveguide feed, so that the measured impedance differs from the actual antenna impedance by only a phase shift factor.)

As one would expect, the data show that much of the incident power is reflected as the feed termination is moved to the edge of the patch in the y direction. There is little variation as the feed is moved along the x direction. Maximum power transfer from a 50 ohm system to the antenna occurs when the feed is terminated at the center of the patch. It should be noted that moving the center of the patch in the positive y direction results in a different impedance than when it is moved in the negative y direction. This indicates that the y directed components of the equivalent magnetic current source may be exciting higher order

modes. The excitation of higher order modes would cause the input impedance to be different.

It is desirable from a circuit designer's point of view to be able to predict the input impedance of the antenna so that the appropriate matching networks can be designed. This is especially important in integrated "active" array applications. The cavity model is a good means for achieving this capability.

Equivalent magnetic current line sources can be placed in the cavity. Modal matching techniques can then be used to find the resulting fields in the cavity. From these fields, total radiated power, dissipated power and stored energy can be calculated in order to predict input impedance. A current distribution on the feed needs to be assumed. The current distribution on an embedded microstrip feed calculated by the moment method could give some insight into the electric current distribution on the center conductor of the coplanar waveguide. This, in turn, could be used to calculate the current distribution of the equivalent magnetic current source.

At this point a computer program based on the cavity model is under development to carry out the calculation of input impedance.

A two-element array (Fig. 4) was constructed and tested to verify the performance of the coplanar waveguide feed in a multielement configuration. Radiation pattern plots (Fig. 5 & Fig. 6) indicate that the coplanar waveguide feeds are coupling power into the antenna. The patterns are also symmetric for this design. More work needs to be done to find the optimum feed network for multiple-element configurations.

Single slot lines (Fig. 7) can also be used to feed the microstrip antenna. To excite the antenna, it is necessary to orient the slot in parallel with a component of the magnetic field of the mode that is to be excited. Figures 8, 9 and 10 give the input impedance and radiation pattern data for a 4.1 GHz slot line fed antenna. Again, a good transition from the 50 ohm coaxial cable to the slot line was constructed so that the measured input impedance of the slot differs from the actual impedance of the antenna by only a phase shift factor. A 1.1:1 input VSWR was achieved at resonance indicating that virtually all the incident power was coupled to the slot line and the antenna.

Several observations should be made on the data. The H plane radiation pattern is asymmetric and the impedance locus does not go to the edge of the Smith chart when the frequency is moved away from the resonant frequency. This suggests that the slot line itself may be radiating. Further experiments will be required to verify this.

One simple experiment that was performed consisted of measuring the return loss versus frequency for both the slot line fed antenna and the short-circuited slot line (2 inches long) with the antenna removed (Fig. 11). For the short-circuited slot line case, a return loss of approximately 3 dB is measured at 4 GHz. This is somewhat greater than what one would expect of a good transmission line (i.e., low loss) with only copper and dielectric losses.

One possible solution to the radiation problem is to use a higher dielectric constant substrate, which will tend to confine the fields. Another possible solution is to configure several slot line fed antennas

in such a way so that the radiation from the feeds is of the proper polarization and does not cause an asymmetry in the radiation patterns.

CHAPTER II.

MEFSET AMPLIFIER DESIGN

In order to integrate the electromagnetically fed microstrip antenna with a MESFET amplifier, it was necessary to design the matching network using a coplanar transmission line rather than microstrip line. Because of the lack of research done in the literature on coplanar discontinuities and matching networks, there were neither design equations (other than equations for impedance and effective dielectric constant) available to design appropriate coplanar elements nor computer-aided design packages such as SUPERCOMPACT or Touchstone to simulate coplanar structures. Therefore, considering the current lack of design tools as well as the narrow-band nature of the patch antenna, a simple narrow-band, 4 GHz maximum available gain (MAG) amplifier was designed rather than a more complicated broadband amplifier network which would have inevitably required some computer-aided design. In addition, the transistor was assumed to be unilateral with source and load impedances equal to 50 ohms though, in general, it should be noted that these impedances are complex.

The design of the MAG amplifier, which was integrated with the electromagnetically fed patch (used as a receiving element), can be summarized in essentially three steps. The first step was to obtain accurate MESFET S-parameters so that stability and conjugate matching impedances can be

determined. The second step was to determine a lumped element prototype which achieves the conjugate matching (assuming 50 ohm input and output impedances) at the MESFET's gate and drain. The third and final step was to replace the lumped elements with various lengths of coplanar transmission lines to approximate the lumped elements.

The MESFET used in the amplifier design was the NEC 700 packaged transistor. Though manufacturer's S-parameters were available, it was decided to measure the transistor's S-parameters due to the sensitivity of maximum gain amplifier design to transistor variation. In order to measure the S-parameters of the FET, a 50 ohm coplanar thru transmission line section was fabricated and its S-parameters measured on the network analyzer. The FET was then placed in the center of the thru line and then biased at a drain voltage of 3 V and drain current of 30 mA (corresponding to the Q point yielding the highest gain). The S-parameters of FET/thru line were then measured on the network analyzer. The S-parameters of the FET were calculated from the FET/thru line data by deembedding the contribution of the thru line. The deembedding was accomplished by first converting the S-parameters into transfer or T-parameters by using the following relations:

$$T_{11} = \frac{1}{S_{21}} \qquad T_{12} = -\frac{S_{22}}{S_{21}}$$

$$T_{21} = \frac{S_{21}}{S_{11}} \qquad T_{22} = S_{12} - \frac{S_{11}S_{22}}{S_{21}}$$

Because T-parameters are cascadable under matrix multiplication, we were able to manipulate the T-matrices and approximately deembed the thru

line from the FET/thru line measurements and, hence, obtain the S-parameter characteristics of the FET only. After obtaining the desired S-parameters, the stability of the FET was calculated at 4 GHz using the following stability criteria

$$K = \frac{1 - |S_{11}|^2 - |S_{22}|^2 + |D|^2}{2|S_{21}\ S_{12}|} > 1 \text{ for stablility}$$

$$\text{where } D = |S_{11}S_{22} - S_{21}S_{12}|$$

The conjugate impedances were also calculated from the S11 and S22 values of the FET with the aid of a Smith chart (16.5 + j66 ohms and 52.5 - j82.5, respectively).

After determining the stablity and the required conjugate matching of the transistor at 4 GHz, a lumped element matching network was calculated using standard Smith chart techniques. Though there are a multitude of matching schemes one could use at this stage, two of the most basic matching networks were developed and optimized on SUPERCOMPACT. The first design (Fig. 12) consisted of series inductors and shunt capacitors. The second design (Fig. 13) consisted of lengths of 50 ohm transmission line and series inductors.

Because the microstrip patch antenna was to be fed electromagnetically via coplanar lines, a coplanar distributed matching network was needed in order to integrate the two devices. As stated earlier, the major problem with distributed coplanar networks is the general lack of design equations with which to approximate lumped elements. There are, however, semiempirical

design equations for the impedance and effective dielectric constant of coplanar lines. Specifically, these equations are

$$\varepsilon_{eff} = [(\varepsilon_r + 1)/2][\tanh\{1.785 \log(h/w) + 1.75\} + \{kW/h\}\{.04 - .7k + .01(1 - .1\varepsilon_0)(.25+k)\}]$$

$$\text{impedance of line} = \frac{30\pi}{\sqrt{\varepsilon_{eff}}} \frac{K'(k)}{K(k)}$$

where K = elliptic integral of the first kind

$K'(k) = K(k')$

$k = \frac{s}{s + 2w}$ $\quad k' = \sqrt{(1 - k^2)}$

w = center conductor to ground spacing

s = width of center conductor

The only matching networks that could be constructed with such limited design equations consist of high impedance and low impedance coplanar transmission lines. It is well known that a length of high impedance line situated between two relatively low impedance lines approximates a series inductor according to the formula

$$\omega L = \frac{z l}{v}$$

where ω = frequency of operation

l = length of line

z = impedance of line

v = effective velocity of line.

Conversely, a low impedance line situated between two relatively high impedance lines approximates a shunt capacitor according to the formula

$$\omega C = \frac{1}{zv}$$

Though it was theoretically possible to realize both our lumped designs on coplanar transmission lines, it turned out that only the design consisting of the series inductors and lengths of transmission line was readily realizable in coplanar form. This result was due to the fact that low impedance lines, i.e., impedances less than 35 ohms, which are needed to approximate shunt capacitors, are very difficult for us to fabricate especially for low dielectric substrates where the center conductor-to-ground distance must be less than 0.125 mm. High impedance lines, i.e., impedances greater than 100 ohms, which are needed to approximate series inductors are, on the other hand, easy to fabricate due to the relatively large center conductor-to-ground distance. Thus, the series inductor/transmission line network was chosen to be realized in the coplanar structure. The choice of the high impedance value to be used was somewhat arbitrary. Though it is known that the inductor approximation improves with higher impedance values, we note that an upper impedance limit exists for a coplanar line of approximately 150 ohms. That is, any impedance greater than 150 ohms will result in the excitation of higher-order non TEM modes. With this limit in mind, a high impedance value of 120 ohms was selected. After having decided what impedances to use, it was necessary to know the effective dielectric constants so that appropriate physical lengths of coplanar lines could be calculated. However, because the design equations are empirically corrected for coplanar lines on high dielectrics, i.e., a di-

electric constant greater than 9, rather than on low dielectrics, which is what we wished to use, 50 ohm and 120 ohm thru lines having the same center conductor width of 3.5 mm were fabricated on 62.5 mil rexolite (dielectric constant of 2.62) using the impedance design equations. They were then measured in the laboratory using time domain reflectometry. By measuring the unit step response of the coplanar lines, we were able to determine the reflection coefficient of the line and, hence, determine the impedance of the line. Then using the following relation,

$$Z = \frac{Z_0(1+\Gamma)}{(1-\Gamma)}$$

where $Z_0 = 50\,\Omega$ = characteristic impedance of source

Γ = reflection coefficient,

we can determine the impedance of the line. According to the step response (Fig. 14) the reflection coefficient of the 50 ohm coplanar line equals -0.02 which corresponds to an impedance of 48 ohms. The reflection coefficient of the 120 ohm coplanar line (Fig. 15) was found to be 0.4 which corresponds to an impedance of 117 ohms. Therefore, the impedance design equation appeared to be valid for low dielectric substrates. To measure the effective dielectric constant of the lines, we needed to measure the impulse response of the lines with short circuits placed at fixed distances along the line. By knowing the impulse response of the line, we could measure, in time, how far apart the short circuits were. Since the distances between the short circuits are known (2 cm), we were able to calculate the velocity of the impulse and, hence, the effective dielectric constant of the line. A-

nalysis of TDR measurements shows that the effective dielectric constants were 1.485 and 1.395 for the 50 ohm and 120 ohm lines, respectively. Comparing the calculated dielectric constants of 1.695 for the 50 ohm case and 1.421 for the 120 ohm case with the TDR measurements, we see good agreement for the 120 ohm case but a rather large discrepancy between the effective dielectric constants for the 50 ohm case. The fact that the measured effective dielectric constants were, in general, less than those predicted by the design equations indicates that the field confinement for the low dielectric case, particularly for the narrow center conductor-to-ground spacing, is less than that predicted by the design equations. It is believed that this difference is caused primarily by the empirical corrections added to the effective dielectric equations. Since the equations were made to fit experimental data obtained for coplanar lines on high dielectric substrates rather on than the low dielectric substrates, it is a likely source of error. For our coplanar design, we used the experimental effective dielectric constants to convert the transmission line/series inductor MAG amplifier matching network into lengths of 50 ohm and 120 ohm coplanar lines.

CHAPTER III.

INTEGRATED "ACTIVE" ARRAY ELEMENT

After designing the transmission line/series inductor amplifier on coplanar transmission lines, a prototype was constructed on 62.5 mil Rexolite (Fig. 18). The amplifier was then tested on the network analyzer and found to have a return loss of 16.7 dB and gain of 9 dB at a frequency of 3.78 GHz (Fig. 16). Though the frequency of operation is slightly off

the design frequency of 4 GHz and the gain is approximately 5 dB less than the maximum available gain, the coplanar matching network has nonetheless improved the performance of the FET. The deviation in performance from theoretical performance is due to the presence of coplanar discontinuities, dc blocking capacitors as well as the biasing network (fig. 18), all of which were either currently unmodelable on the computer or assumed to have negligible effect on the matching network.

After measuring the amplifier by itself, the amplifier was integrated with a single microstrip patch (operating frequency of 3.78 GHz). The patch was placed on the uncladded side of the Rexolite substrate over a length of 50 ohm coplanar line which extended from the matching network (fig. 18). In order to satisfy the 50 ohm source assumption used in the amplifier design, the input impedance of the patch antenna at various coplanar feed points was determined by measuring the return loss of the patch versus feed location (Table 1). A feed location with an optimum return loss of 16.0 dB was found. Since such a return loss did not represent a perfect 50 ohm line, a mismatch loss given by

$$\text{Mismatch Loss} = 10 \log \frac{P_{del}}{P_{av}} = 10 \log \left[\frac{(1 - |\Gamma_L|^2)(1 - |\Gamma_S|^2)}{|1 - |\Gamma_L||\Gamma_S| \exp j(\theta_L + \theta_S)|^2} \right]$$

where $|\Gamma_L|$ = reflection coefficient at antenna

$|\Gamma_S|$ = relection coefficeint of the amplifier

P_{del} = power delivered

P_{av} = power available

was expected to reduce the gain of the amplifier.

The radiation pattern for the integrated "active" element is given in Figs. 19, 20. It is superimposed on the radiation pattern of a "passive" element with the same feed structure but no amplifier. The difference in power levels indicates that the amplifier adds approximately 13 dB of gain of the antenna element. The ripple in the radiation pattern of the integrated element is due to the effects of diffraction at the edges which were magnified by the use of a large but finite ground plane on which the the element was fabricated. A smaller ground plane, which reduces the diffraction effects, was used for the pattern measurement of the antenna element alone and found to reduce the ripple. One notes that, unlike the H-plane pattern, the E-plane radiation pattern demonstrates a slight asymmetry. This asymmetry is attributed to the presence of the coplanar feed and amplifier which lie on the same axis.

In the future, work will be focused on refining the integration design procedure by eliminating the need to resort to empirical design data while improving the overall performance characteristics of the integrated antenna/amplifier. In particular, a computer program based on theoretical analysis will be developed which will calculate the input impedance of the coplanar and slot line feed patch antennas. Work on characterizing novel coplanar line configurations will also be done so that a more compact, broader band amplifier can be constructed which will

not only minimize the asymmetry in the radiation pattern, but facilitate multielement antenna/amplifier integration. Finally, attention will be focused on designing integrable coplanar feed networks which can be used in the fabrication of large multielement antenna/amplifier arrays.

TABLE 1

INPUT REFLECTION COEFFICIENT VERSUS FEED LOCATION FOR COPLANAR FEED MICROSTRIP ANTENNA

Δx (cm)	Δy (cm)	$20 \log \lvert\Gamma_{in}\rvert$ (db)
0	1.000	-4.5
0	0.875	-4.9
0	0.750	-7.9
0	0.500	-11.6
0	0	-16.0
0	-.0250	-11.8
0	-0.500	-5.8
0	-1.000	-1.6
0.250	0	-13.6
0.500	0	-14.2

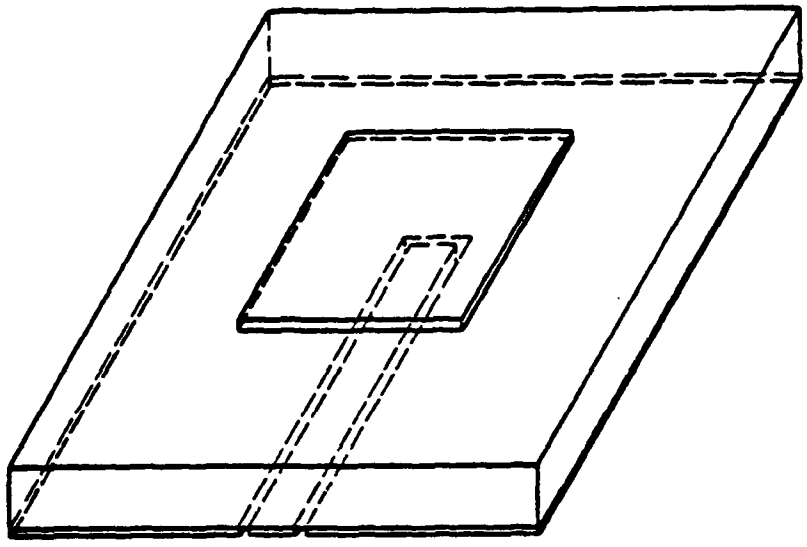

Figure 1. Microstrip antenna element with coplanar waveguide feed.

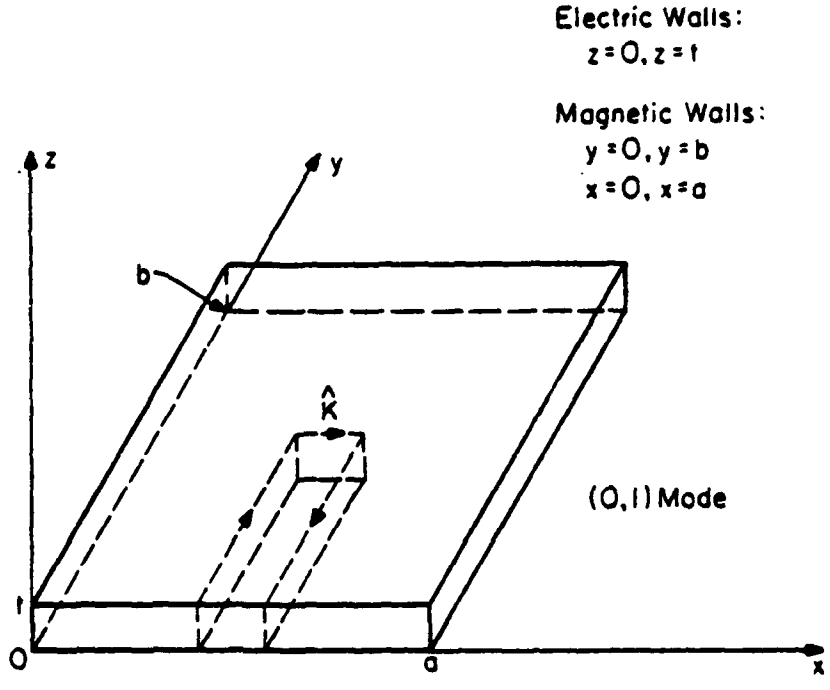

Figure 2. Cavity model representation of microstrip antenna element with coplanar waveguide feed.

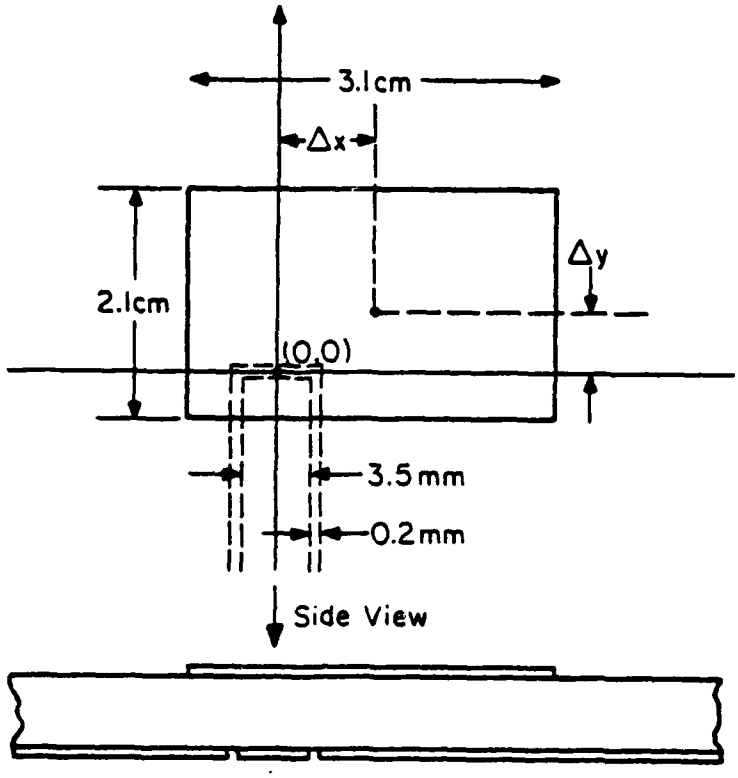

Substrate: 1/16" Thick Rexolite 2200, $\epsilon_r = 2.62$
$f_{meas} = 4.1$ GHz

Figure 3. Definition of coordinates used to describe the location of the microstrip antenna element feed point.

Substrate: Rexolite 2200, $\epsilon_r = 2.62$

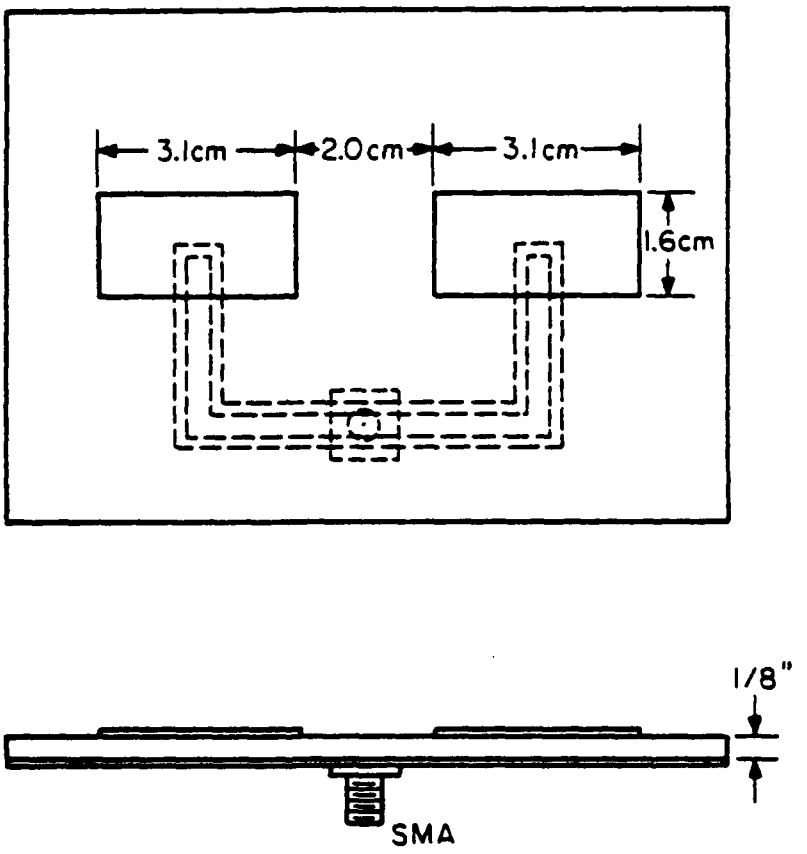

Figure 4. Two element, coplanar feed, microstrip antenna array. (f = 4.5 GHz)

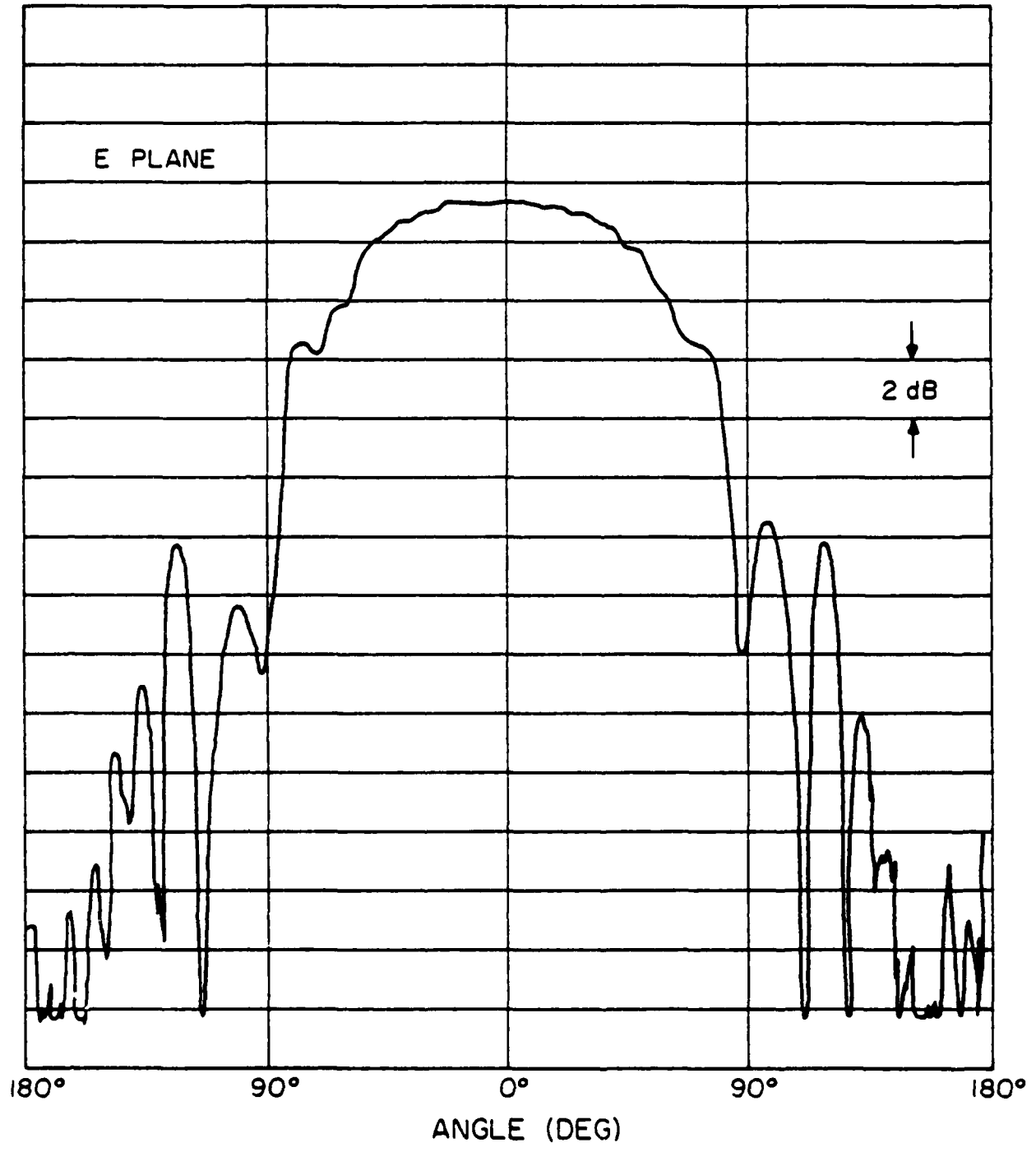

Figure 5. Two element array radiation pattern - E-plane. (Coplanar waveguide feed) (f = 4.5 GHz)

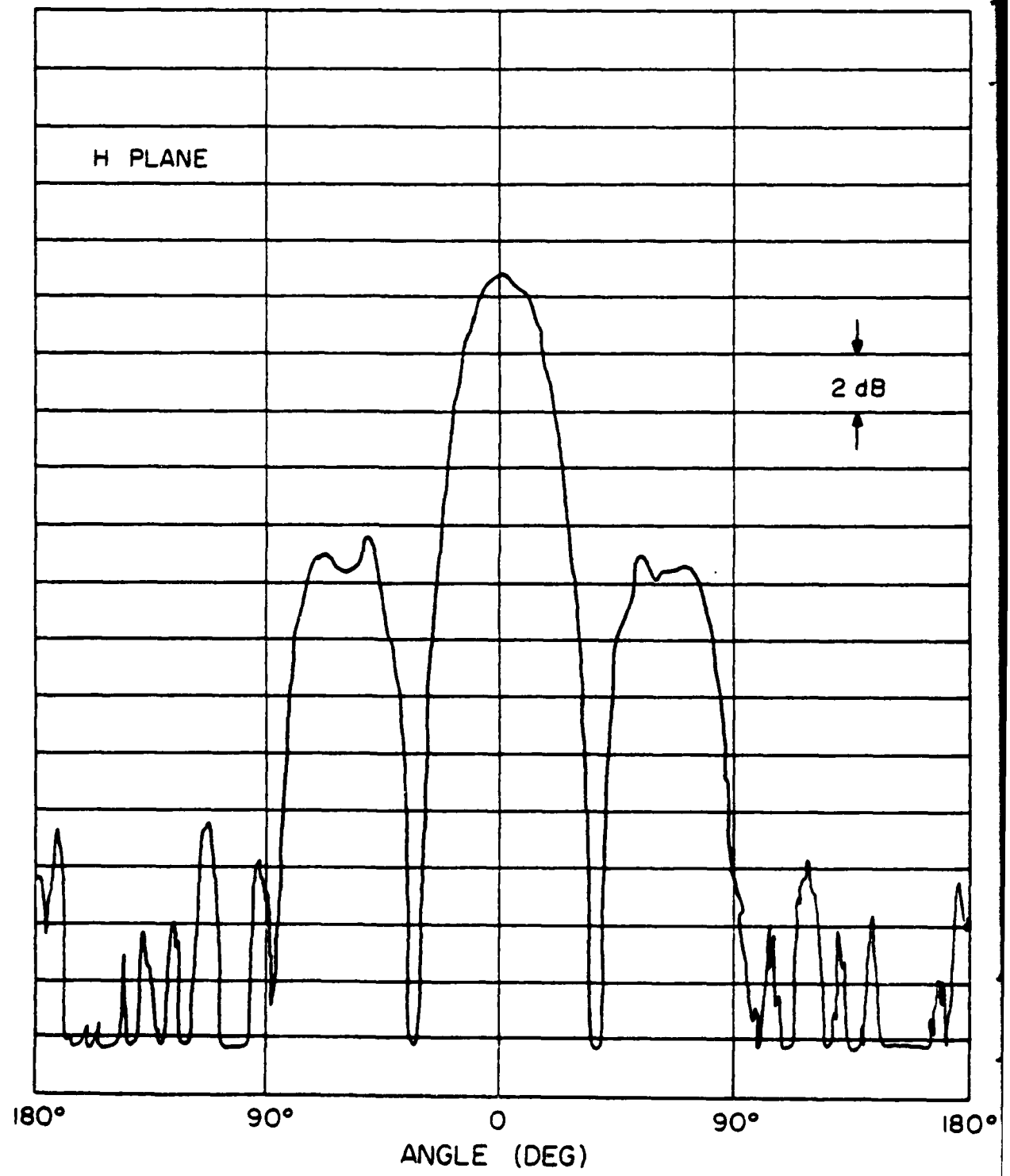

Figure 6. Two element array radiation pattern - H-plane. (Coplanar waveguide feed) (f = 4.5 GHz)

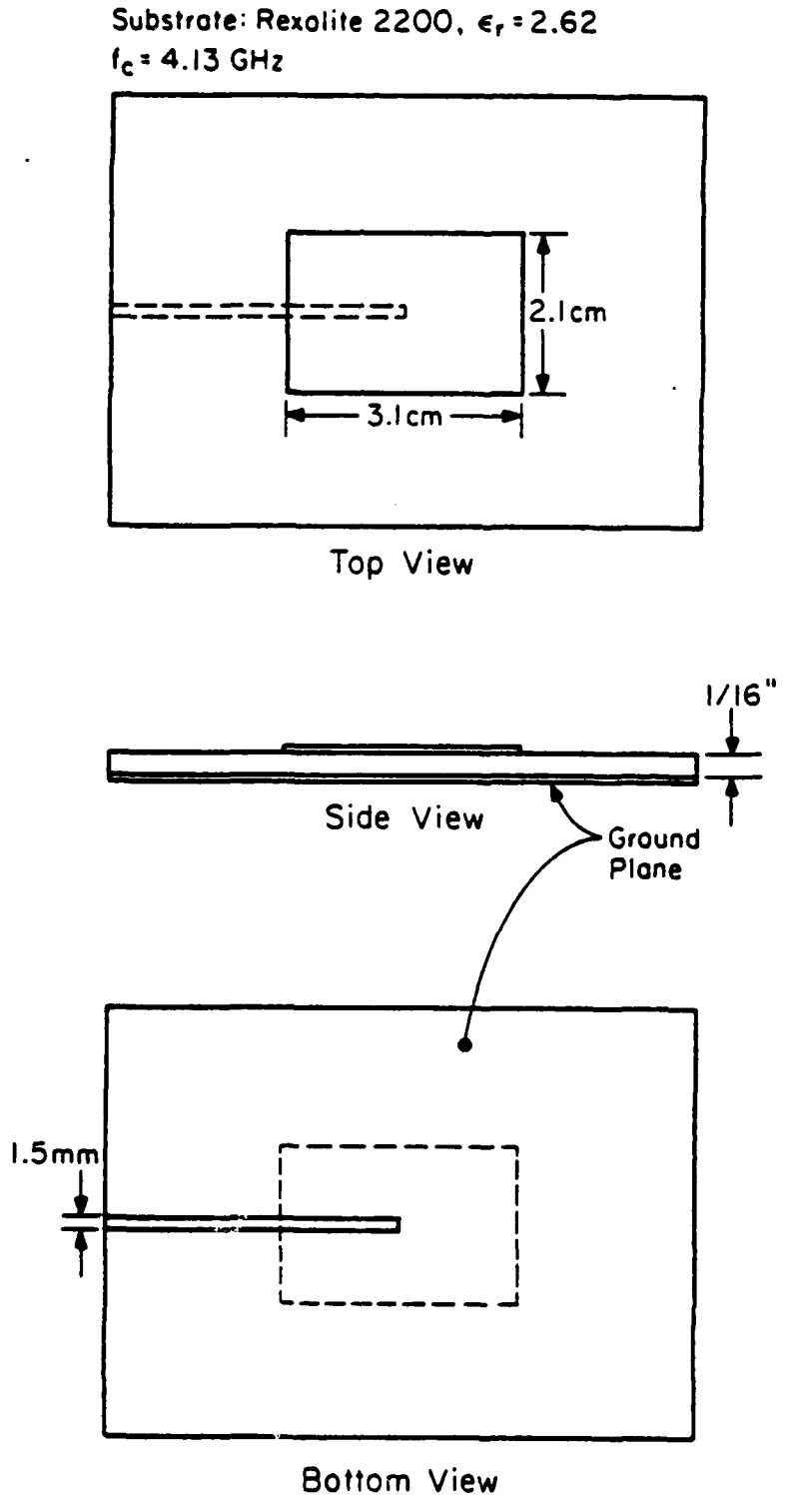

Figure 7. Microstrip antenna element with electromagnetically coupled slot line feed.

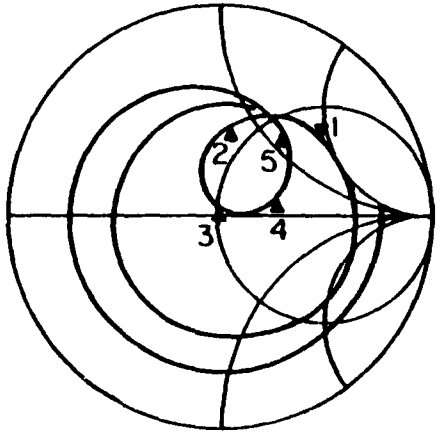

Marker	Frequency (GHz)
1	4.3
2	4.2
3	4.1
4	4.0
5	3.9

(a)

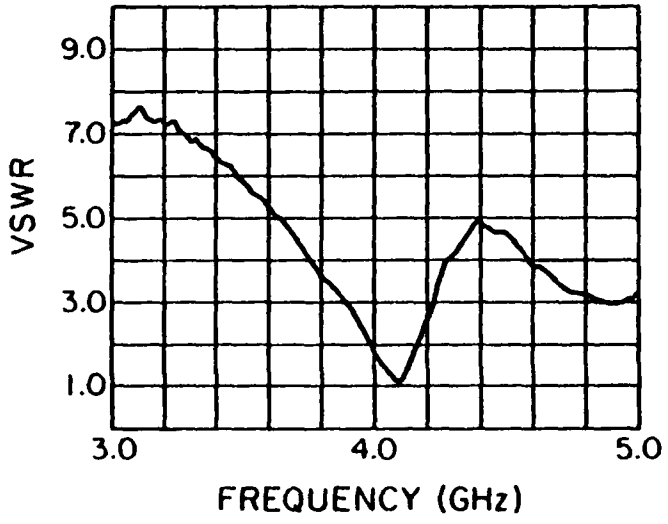

(b)

Figure 8. Microstrip antenna element with slot line feed.
a) Element input impedance (z) versus frequency.
b) Element input VSWR versus frequency.

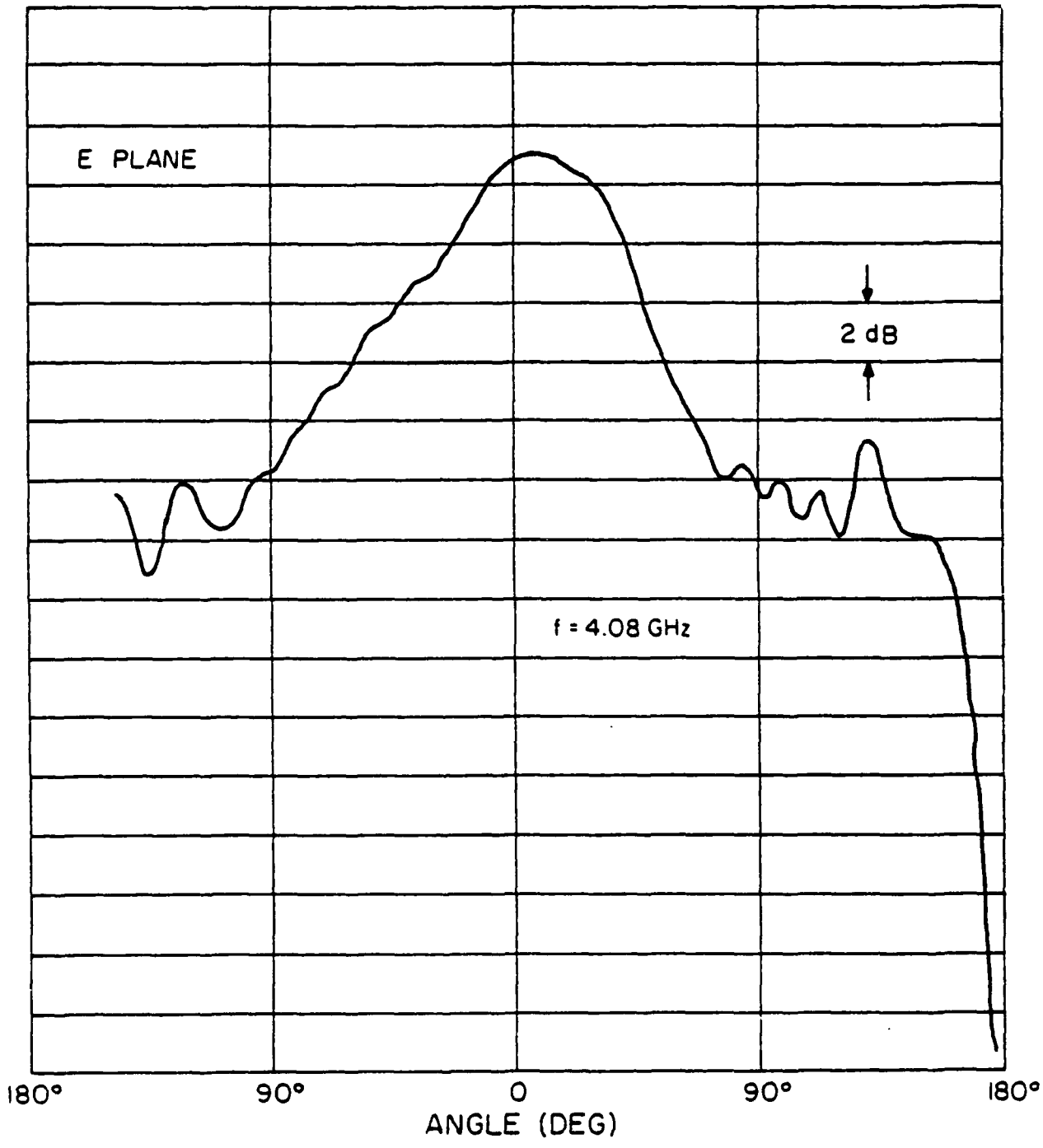

Figure 9. Radiation pattern of element with slot line feed. (E-plane)

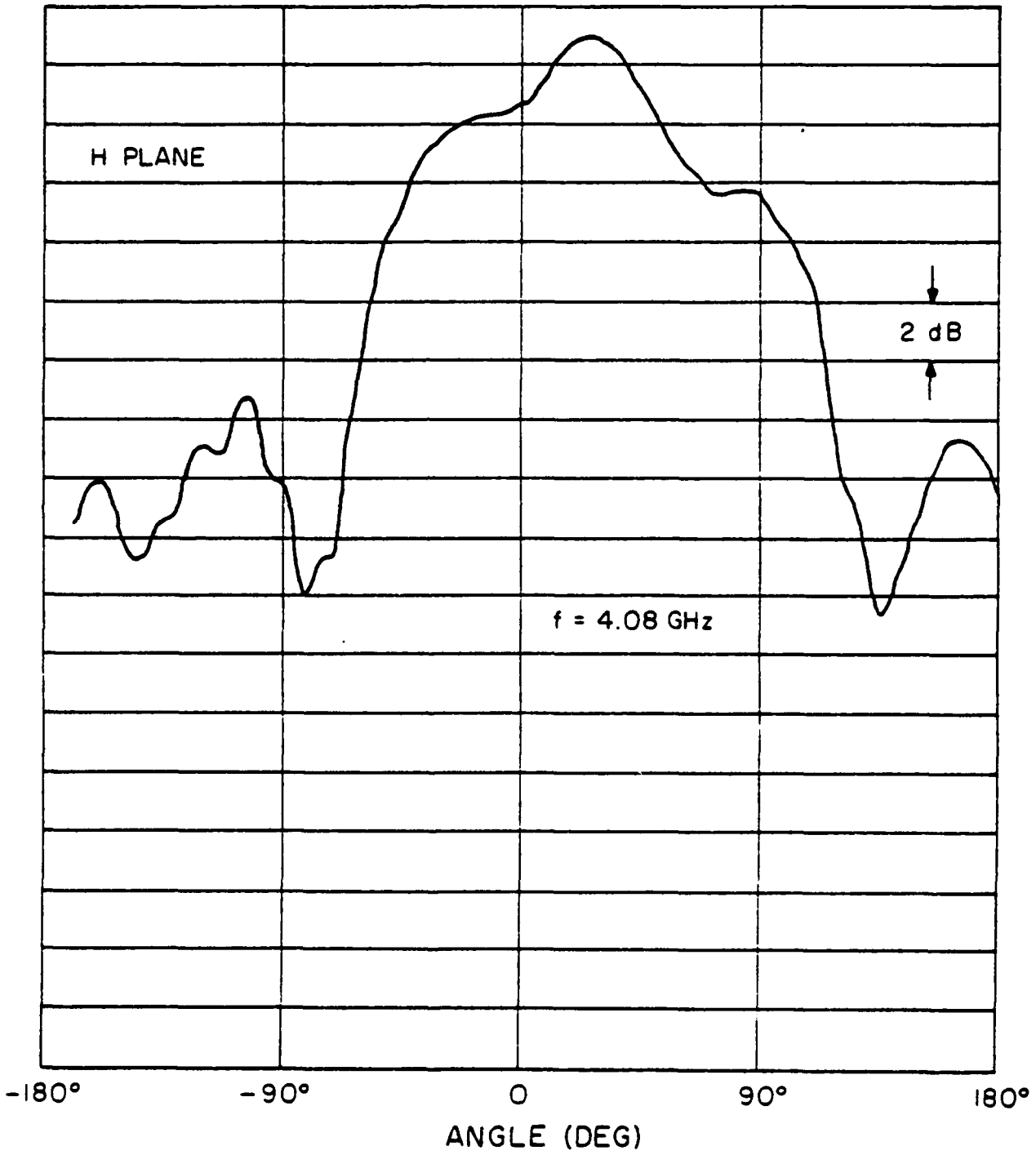

Figure 10. Radiation pattern of element with slot line feed. (H-plane)

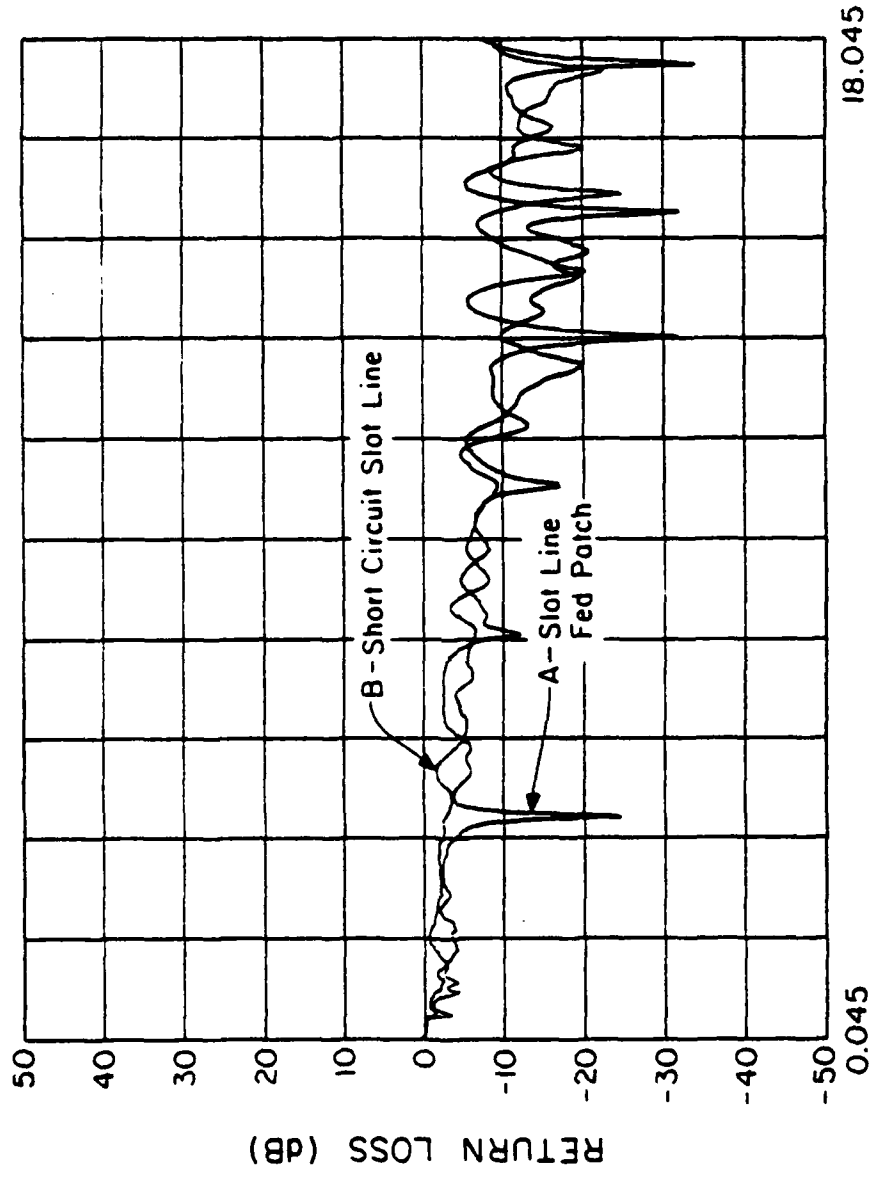

Figure 11. Return loss of slot line fed patch (A) and short circuited slot line (B).

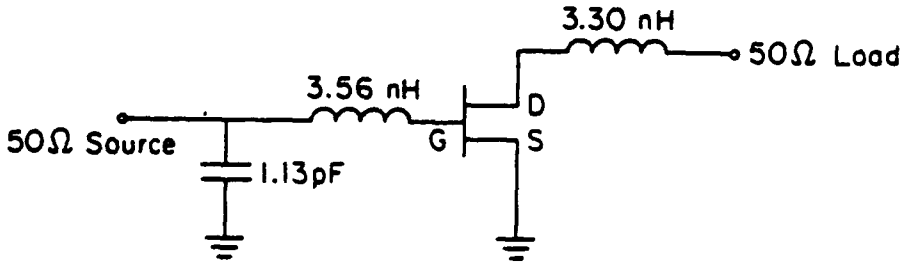

Figure 12. Amplifier design #1.

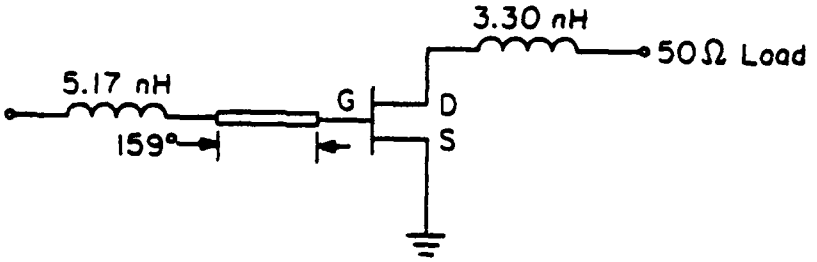

Figure 13. Amplifier design #2.

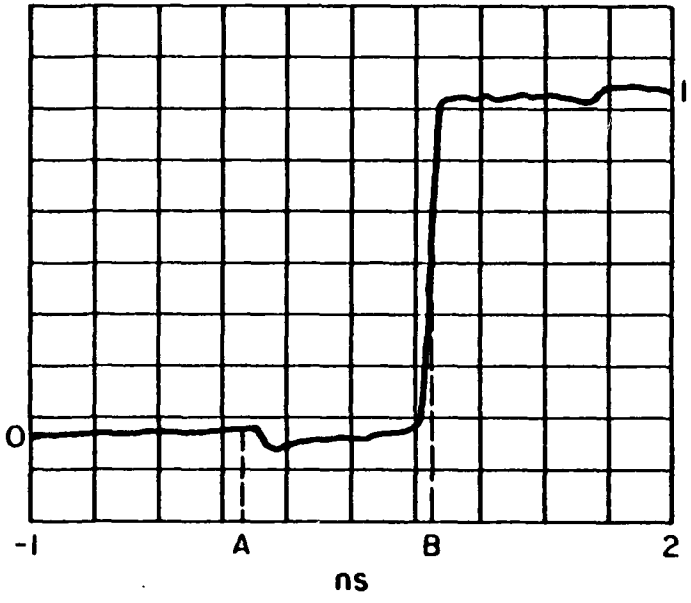

A — 50Ω Coaxial Cable to 50Ω Coplanar Waveguide Transition

B — Open Circuit Termination

Figure 14. Step response of 50 Ω coplanar waveguide.

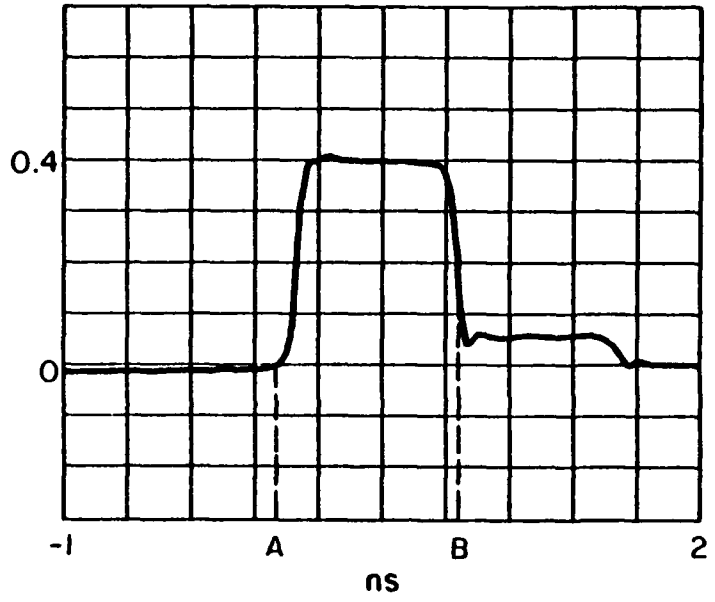

A — 50Ω Coaxial Cable to 120Ω Coplanar Waveguide Transition

B — 50Ω Termination

Figure 15. Step response of 120 Ω coplanar waveguide.

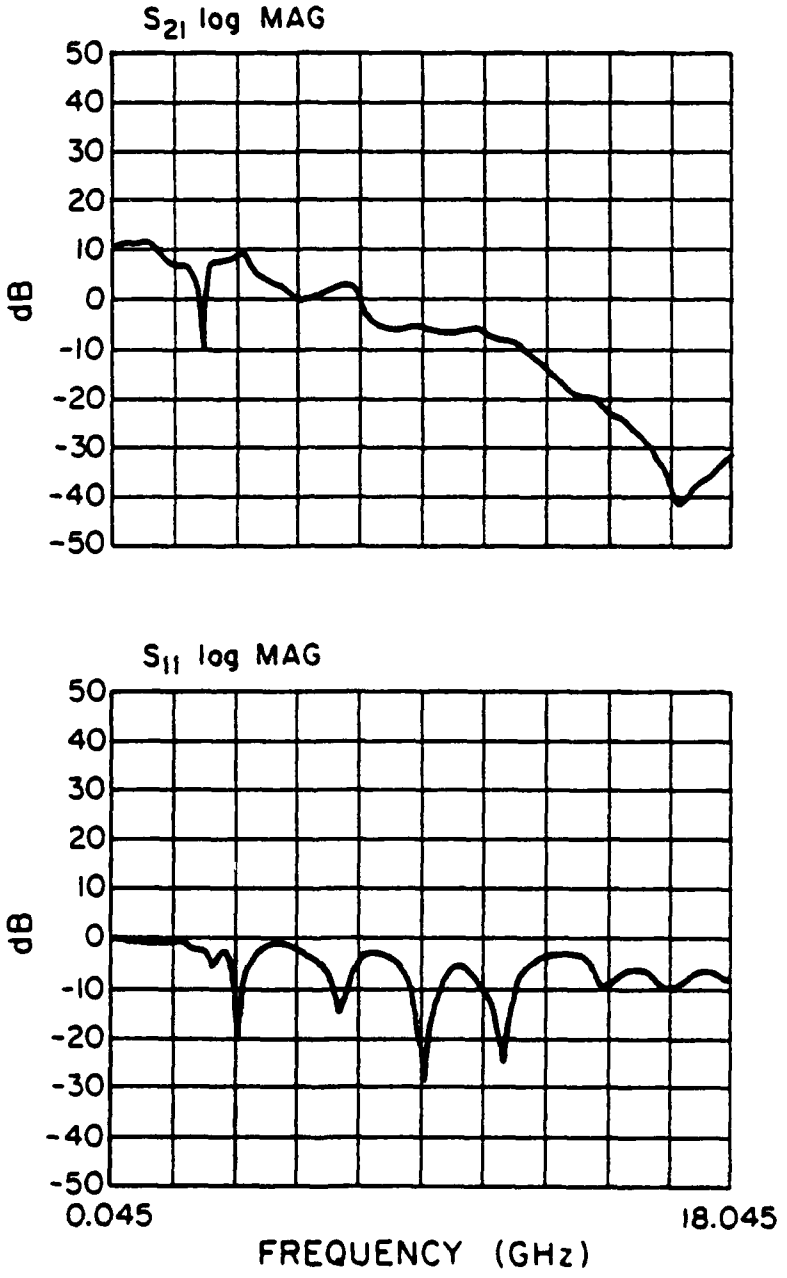

Figure 16. Frequency response of prototype amplifier #1.

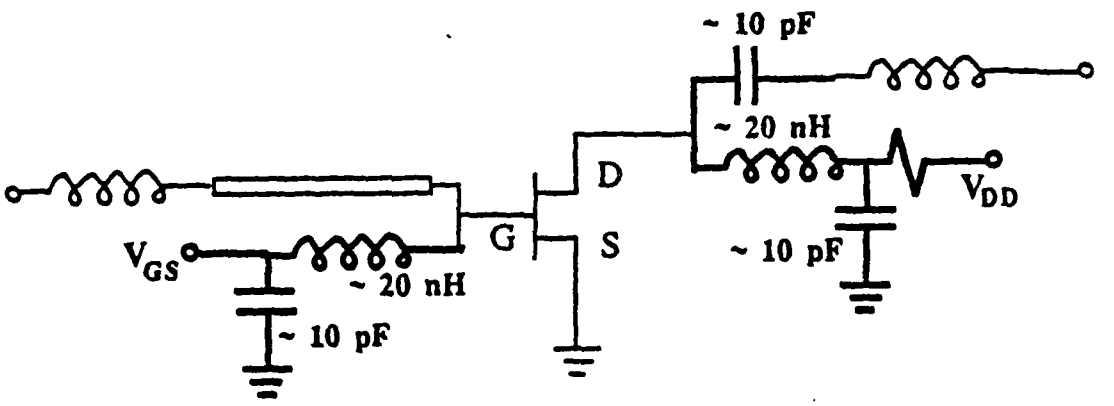

Figure 17. Amplifier design with bias network emphasized.

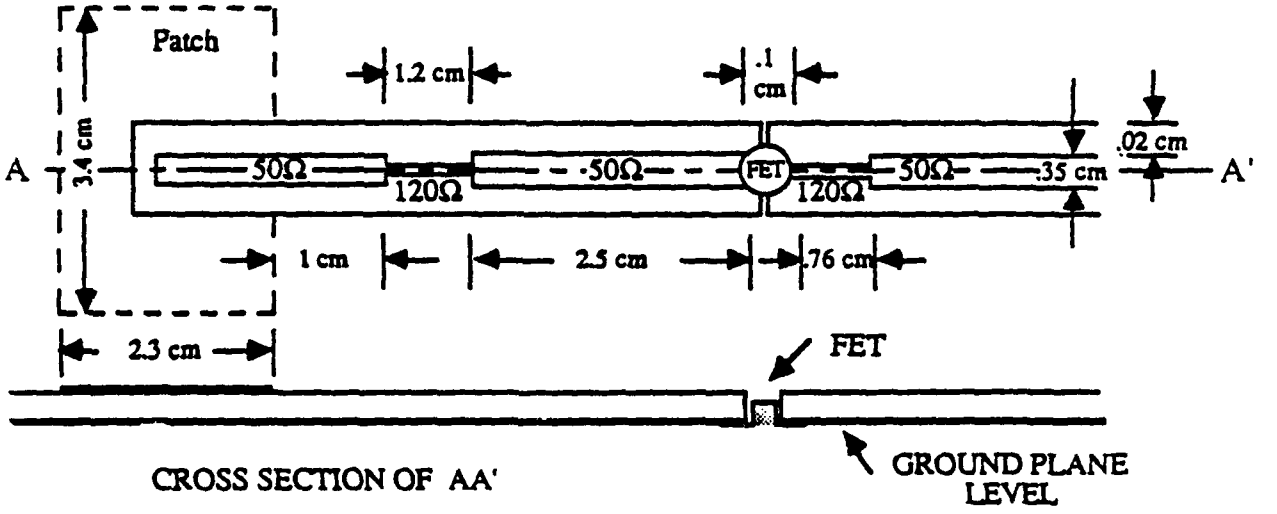

Figure 18. "Active" microstrip antenna element.

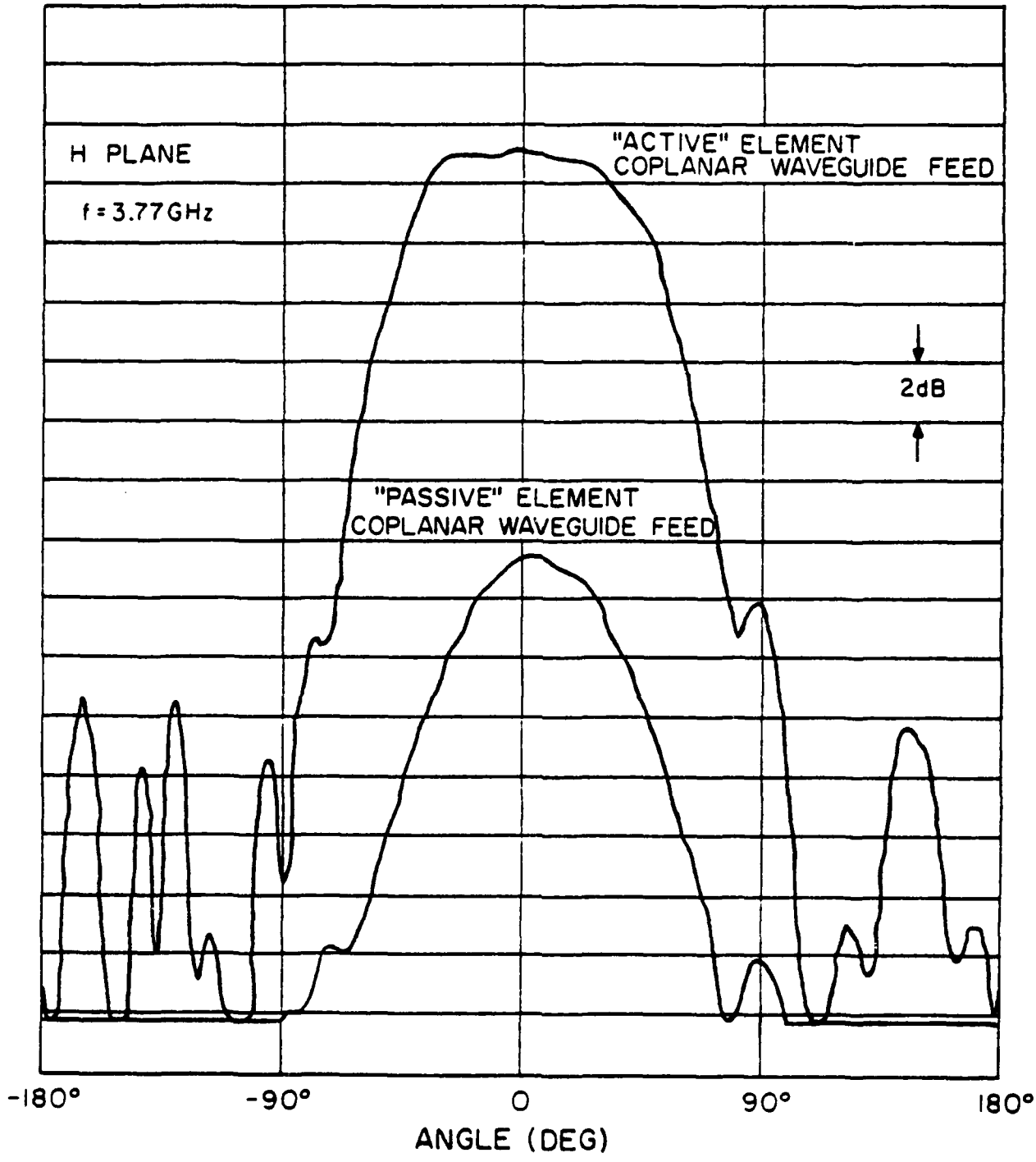

Figure 19. Radiation patterns for "active" and "passive" microstrip antenna elements. (H-plane)

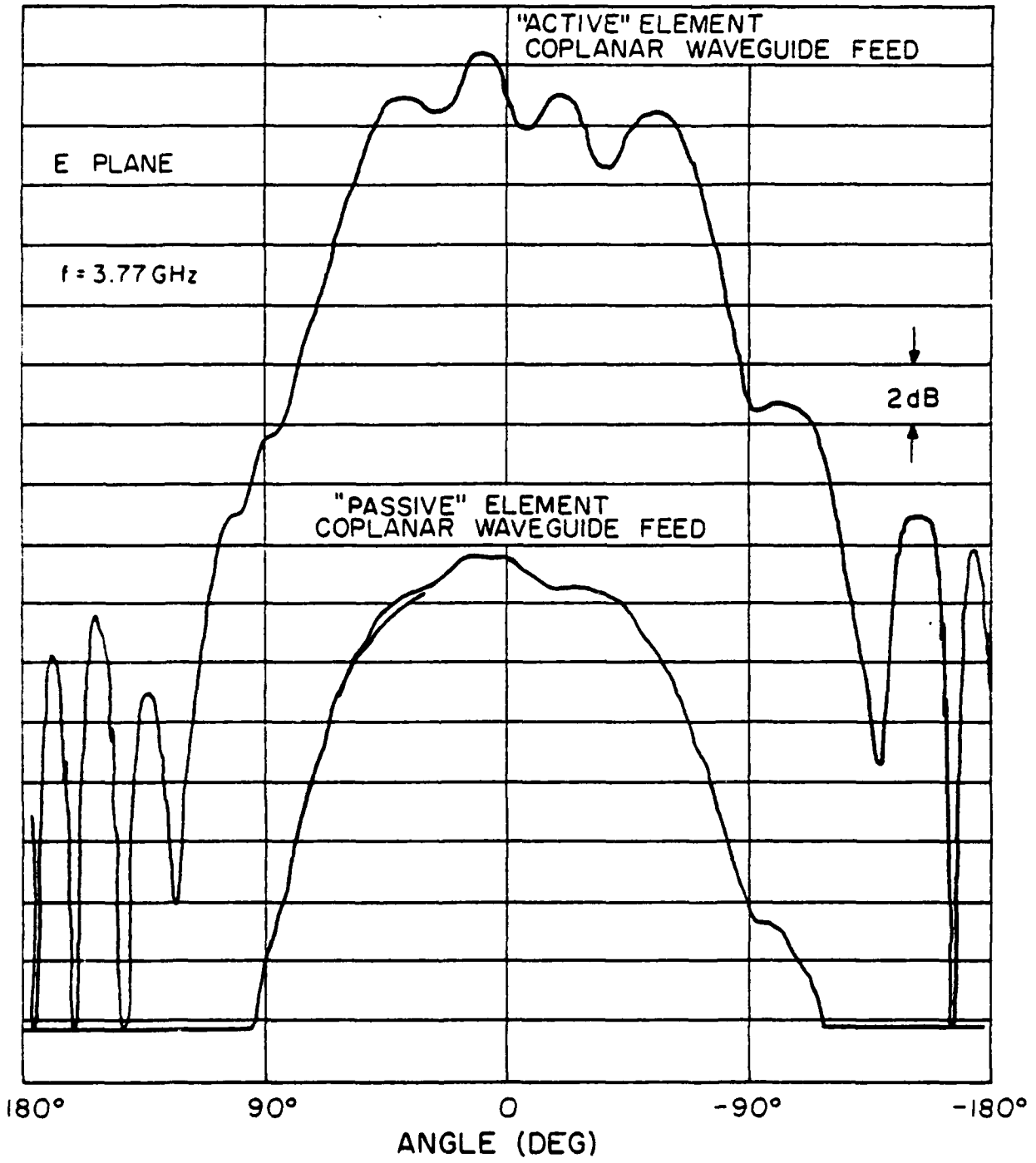

Figure 20. Radiation patterns for "active" and "passive" microstrip antenna elements. (E-plane)

CHAPTER IV

RIGOROUS ANALYSIS OF A CIRCULAR PATCH ANTENNA EXCITED BY A MICROSTRIP TRANSMISSION LINE

M. Davidovitz

Y.T. Lo

ABSTRACT

Circular patch antenna excited by a microstrip transmission line is analyzed. Boundary conditions are enforced on a portion of the microstrip feed line as well as the patch antenna. The integral equation for the unknown currents on the antenna and the feed is solved by applying the Galerkin method of moments in the Fourier Transform domain. A method designed to accelerate the convergence of the resulting spectral integrals is outlined and discussed. Extensive input impedance data are presented for the case of the electromagnetically coupled circular patch. The accuracy of the computed results is verified experimentally.

I. INTRODUCTION

Microstrip antennas have been analyzed extensively in the past decade, employing a wide variety of analytical techniques, ranging from the simple intuitive models to rigorous numerical treatments. Oftentimes, in order to make the computations more tractable, simplifying assumptions about the feed were introduced into the formulation. This placed restrictions on the range of validity of the models in question. Specifically, probe and microstrip transmission line feeds were in many instances modeled by current filaments.

Aside from the fact that such idealizations are not adequate for thicker elements, they cannot be applied for more complicated feeding arrangements. Particularly, in the case of the electromagnetic coupling or proximity feed it is clear that boundary conditions on at least a portion of the microstrip line must be accounted for in the formulation.

This paper undertakes the analysis of the circular patch antenna excited by a microstrip transmission line. The method presented is applicable to all microstrip line feeding arrangements, including the edge feed, capacitive gap feed and the proximity or coupling feed. The problem is formulated in the Fourier Transform (FT) domain. Moment Method is applied to solve the integral equation for the currents on the patch and portion of the feed line. Considerable attention is given to acceleration of convergence of the Sommerfeld-type integrals which arise in the course of the analysis.

In Section II the integral equation for the unknown patch and microstrip feed line currents is formulated. The derivation is performed in the FT domain and utilizes the dyadic Green function for the multilayered grounded dielectric slab. A set of basis-testing functions is introduced for the patch and microstrip line. Parseval's theorem is applied to implement the Galerkin Moment Method solution in the FT domain. The resulting matrix elements take the form of improper single or double integrals.

Section III outlines and discusses a method to accelerate the convergence of the improper integrals. The idea behind the method is similar to singularity subtraction in evaluation of singular

integrals. It involves subtraction of the slowly decaying terms of the integrand, which due to their simple form can be readily evaluated. This procedure tends to increase the efficiency and accuracy[1] of the computation.

The degree of accuracy to which the input impedance can be computed depends to a large extent on the model of the excitation mechanisms. In Section IV a unit voltage source is introduced on the microstrip transmission line. Input impedance is defined based on the transmission line model of the actual physical configuration.

Theoretically computed results are compared with experimental data in Section V. Since virtually no data exists on proximity fed circular patches, efforts are concentrated in that direction. Results are exhibited for a number of configurations.

Finally, discussion and conclusions are presented in Section VI.

---

1. Note, the ultimate test of accuracy is comparison of computed results with experimental data.

II. FORMULATION OF THE PROBLEM

There exist several equivalent ways of deriving the dyadic Green function for the multilayered grounded dielectric slab. The present approach utilizes the modal decomposition of the fields transverse to $\hat{\mathbf{z}}$ into E(TM) and H(TE) components. The original three-dimensional problem is thereby reduced to a one-dimensional transmission line problem. This procedure is detailed elsewhere [1]; the resulting equations are summarized below.

To facilitate the following presentation of the dyadic Green function, several necessary definitions are introduced. The FT relations used throughout the paper are:

$$F\{\mathbf{A}(\boldsymbol{\rho},z)\} = \tilde{\mathbf{A}}(\mathbf{k}_t,z) = \iint_{-\infty}^{\infty} \mathbf{A}(\boldsymbol{\rho},z)e^{j\mathbf{k}_t\cdot\boldsymbol{\rho}}\,d\boldsymbol{\rho} \tag{1a}$$

$$F^{-1}\{\tilde{\mathbf{A}}(\mathbf{k}_t,z)\} = \mathbf{A}(\boldsymbol{\rho},z) = \frac{1}{(2\pi)^2}\iint_{-\infty}^{\infty} \tilde{\mathbf{A}}(\mathbf{k}_t,z)e^{-j\mathbf{k}_t\cdot\boldsymbol{\rho}}\,d\mathbf{k}_t \tag{1b}$$

where $\mathbf{k}_t$ is the transverse vector wavenumber, e.g., in the Cartesian coordinate system

$$\mathbf{k}_t = k_x\hat{\mathbf{x}} + k_y\hat{\mathbf{y}} = k_t(\cos\alpha\ \hat{\mathbf{x}} + \sin\alpha\ \hat{\mathbf{y}})\ ;\ k_t^2 = k_x^2 + k_y^2 \tag{2}$$

The corresponding unit vector will be denoted by $\hat{\mathbf{k}}_t$.

Consider a transverse electric current distribution situated in a stratified medium with layers perpendicular to the $\hat{\mathbf{z}}$ axis. The FT of the dyadic Green function for this configuration takes on the following form:

$$\tilde{\tilde{\mathbf{G}}}(\mathbf{k}_t;z,z') = -V'(z,z')\hat{\mathbf{k}}_t\hat{\mathbf{k}}_t - V''(z,z')(\hat{\mathbf{k}}_t\times\hat{\mathbf{z}})(\hat{\mathbf{k}}_t\times\hat{\mathbf{z}}) + \frac{k_t}{\omega\epsilon}I'(z,z')\hat{\mathbf{z}}\hat{\mathbf{k}}_t \tag{3}$$

$V'(z,z')$ and $V''(z,z')$ are, respectively, the E- and H-mode characteristic Green functions, satisfying the following set of transmission line equations

$$\frac{d}{dz}V(z,z') + jk_zZI(z,z') = 0 \tag{4a}$$

$$\frac{d}{dz}I(z,z') + jk_zYV(z,z') = i \tag{4b}$$

where $i = \delta(z-z')$ or $i=0$ depending on whether the source point z' and the observation pont z are or are not in the same stratum. Furthermore:

$$Z' = 1/Y' = k_z/\omega\epsilon \quad . \qquad \text{E—modes} \tag{5a}$$

$Z =$

$$Z'' = 1/Y'' = \omega\mu/k_z \quad . \qquad \text{H—modes} \tag{5b}$$

$$k_z = \sqrt{k^2-k_t^2}; \; k^2 = \omega^2\mu\epsilon \tag{5c}$$

The branch of the square root in equation (5c) is chosen such as to satisfy the radiation condition for the assumed $e^{j\omega t}$ time dependence.

As an example illustrating the solution of equations (5a.b) consider the case of a two-layer slab backed by a ground plane. Figure 1 shows the physical configuration alongside the equivalent transmission line model. The dielectric layers are characterized by their permittivities ϵ_1, ϵ_2 and respective thicknesses t_1, t_2. The source point z' is located in the second layer, i.e. $z_1 \leqslant z' \leqslant z_2$. The characteristic Green function for this example is given by:

$$V_2(z_2,z')\, e^{-jk_{z0}(z-z_2)} \qquad z_2 \leqslant z \tag{6a}$$

$$V(z,z') = \quad V_2(z,z') \qquad z_1 \leqslant z \leqslant z_2 \tag{6b}$$

$$V_2(z_1,z')\, \frac{\sin(k_{z1}z)}{\sin(k_{z1}z_1)} \qquad 0 \leqslant z \leqslant z_1 \tag{6c}$$

where

$$V_2(z,z') = \frac{1}{\overleftrightarrow{Y}'(z_1)}[\cos k_{z2}(z_<-z_1) + j\overleftrightarrow{Y}'(z_1)\sin k_{z2}(z_<-z_1)] \times$$

$$\times [\cos k_{z2}(z_>-z_1) - j\overleftrightarrow{Y}'(z_1)\sin k_{z2}(z_>-z_1)] \tag{7a}$$

$$\left.\begin{aligned} \vec{Y}'(z_1) &= \frac{Y_2 - jY_0\cot(k_{z2}t_2)}{Y_0 - jY_2\cot(k_{z2}t_2)} \quad ; \vec{Y}(z_1) = Y_2\vec{Y}'(z_1) \\ \overleftarrow{Y}'(z_1) &= -j\frac{Y_1}{Y_2}\cot(k_{z1}t_1) \quad ; \overleftarrow{Y}(z_1) = Y_2\overleftarrow{Y}'(z_1) \end{aligned}\right\} \tag{7b}$$

$$\overleftrightarrow{Y}(z_1) = \overleftarrow{Y}(z_1) + \vec{Y}(z_1). \tag{7c}$$

and

$$z_{\gtrless} = \begin{cases} z, & z \gtrless z' \\ z', & z' \gtrless z \end{cases}$$

Note, equations (4,6,7) are equally valid for both E- and H-mode characteristic Green functions. $V''(z,z')$ or $V''(z,z')$ are obtained from (6.7) by substitution of the respective modal admittances Y' or Y'', given by (5).

Formulation of the integral equation for the unknown currents on the patch and feedline, $\mathbf{J}_p$ and $\mathbf{J}_l$, respectively, can be carried out with the aid of the Green function given by equations (3-7). Enforcement of the boundary condition requiring the total tangential electric field to vanish on the microstrip patch and line, yields the sought integral equation

$$\hat{\mathbf{z}} \times \left[\mathbf{E}^i(\mathbf{r}) + \mathbf{E}(\mathbf{r})\right] = 0 \quad \mathbf{r} \in \left[S_p + S_l\right]$$

where $\mathbf{E}^i(\mathbf{r})$ denotes the impressed or incident electric field and

$$\mathbf{E}(\mathbf{r}) = \int\int_{S_p} \bar{\bar{\mathbf{G}}}(\mathbf{r},\mathbf{r}') \cdot \mathbf{J}_p(\mathbf{r}')d\mathbf{r}' + \int\int_{S_l} \bar{\bar{\mathbf{G}}}(\mathbf{r},\mathbf{r}') \cdot \mathbf{J}_l(\mathbf{r}')d\mathbf{r}' \tag{8a}$$

$$= F^{-1}\left[\tilde{\bar{\bar{\mathbf{G}}}}(\mathbf{k}_t;z,z') \cdot \mathbf{J}_p(\mathbf{k}_t)\right] + F^{-1}\left[\tilde{\bar{\bar{\mathbf{G}}}}(\mathbf{k}_t;z,z') \cdot \mathbf{J}_l(\mathbf{k}_t)\right] \tag{8b}$$

Equation (8b) is obtained from (8a) by extending the domains of integration S_p and S_l, shown in Figure 2, to the entire plane and applying basic FT relations.

Galerkin's method of moments is implemented in the FT domain to reduce the integral equation (8b) to a matrix equation. The accuracy and efficiency of the solution largely depends upon

the choice of the expansion and testing functions. This choice can be guided by previous investigations of related geometries, and dictated by the inherent features of the configuration, such as symmetries, edges, etc., as well as numerical considerations. The selection of the expansion-testing functions for the problem at hand is based upon the previous work of several authors [2,3,4].

The currents on the circular patch of radius c are represented by the following set of basis functions:

$$\mathbf{J}_\rho = \sum_{m,\nu} I^\rho_{m\nu}\,\mathbf{J}^\rho_{m\nu} + \sum_{n,\xi} I^\phi_{n\xi}\,\mathbf{J}^\phi_{n\xi} \qquad m,\nu,n,\xi = 0,1,2,\ldots\ ,\quad m+\nu, n+\xi \text{ odd} \tag{9a}$$

$$\text{where } \mathbf{J}^\rho_{m\nu} = \hat{\boldsymbol{\rho}}\,P_\nu(\rho/c)\cos(m\phi);\ P_\nu(\rho/c) = U_\nu(\rho/c)\sqrt{1-(\rho/c)^2} \tag{9b}$$

$$\mathbf{J}^\phi_{n\xi} = \hat{\boldsymbol{\phi}}\,\Phi_\xi(\rho/c)\sin(n\phi);\Phi_\xi(\rho/c) = T_\xi(\rho/c)/\sqrt{1-(\rho/c)^2} \tag{9c}$$

T_ξ, U_ν are Cheybishev polynomials of first and second kind, respectively. These basis functions are particularly suitable for problems involving the circular disc because they correctly model the behavior of the currents near its edge. In addition they possess a closed form Fourier-Bessel transforms, which are given by

$$\tilde{\mathbf{J}}^\rho_{m\nu} = \pi j^{m+1}\left\{\mathbf{k}_t\cos(m\alpha)U^-_{m,\nu}(k_t c/2) - (\mathbf{k}_t\times\hat{\mathbf{z}})\sin(m\alpha)U^+_{m,\nu}(k_t c/2)\right\} \tag{10a}$$

$$\tilde{\mathbf{J}}^\phi_{n\xi} = \pi j^{n+1}\left\{\mathbf{k}_t\cos(n\alpha)T^+_{n,\xi}(k_t c/2) - (\mathbf{k}_t\times\hat{\mathbf{z}})\sin(n\alpha)T^-_{n,\xi}(k_t c/2)\right\} \tag{10b}$$

Functions $U^\pm_{m,\nu}(k_t c/2)$, $T^\pm_{n,\xi}(k_t c/2)$ can be found in Appendix A.

The current on the microstrip transmission line of width 2w is approximated by a subsectional basis set consisting of the following functions

$$\mathbf{J}_l = \hat{\mathbf{x}}\sum_n I^x_n J^x_n = \hat{\mathbf{x}}\sum_n I^x_n T_n(x)P(2w) \tag{11a}$$

where

$$T_n(x) = \left| 1 - \frac{|x - x_n|}{\Delta} \right| : \quad x_n - \Delta \leq x \leq x_n + \Delta \tag{11b}$$

$$P(2w) = \begin{cases} \frac{1}{2w} & -w \leq y \leq w \\ 0 & \text{otherwise} \end{cases} \tag{11c}$$

with w as shown in Figure 2. The FT of J_n^x is readily shown to be

$$\tilde{J}_n^x = J_x e^{jk_x x_n} = \left\{ \Delta \frac{\sin^2\left|\frac{k_x\Delta}{2}\right|}{\left|\frac{k_x\Delta}{2}\right|^2} \frac{\sin(k_y w)}{(k_y w)} \right\} e^{jk_x x_n} \tag{12}$$

Next, the moment method matrix is formulated using the basis-testing functions introduced above. Both expansion and testing take place in the FT domain, the latter with the aid of the following Parseval's Theorem

$$\iint_S \mathbf{E}(\boldsymbol{\rho},z) \cdot \mathbf{J}(\boldsymbol{\rho},z) ds = \int_{-\infty}^{\infty} \tilde{\mathbf{E}}(\mathbf{k}_t,z) \cdot \tilde{\mathbf{J}}^*(\mathbf{k}_t,z) \frac{d\mathbf{k}_t}{(2\pi)^2} \tag{13}$$

The resulting matrix can be partitioned into three distinct submatrices. One of the submatrices, itself of a block diagonal form, represents the interaction between the various current modes on the patch. Another serves the same purpose for the microstrip line and possesses a Toeplitz structure. The third couples the patch current modes to the microstrip line. Tabulation of the various types of elements can be found in Table I.

To recapitulate, the Green function for the stratified dielectric slab backed by a ground plane was used to formulate the integral equation for the currents on the patch antenna and microstrip feedline. A set of expansion-testing functions was introduced and Galerkin's method of moments applied to reduce the problem to a set of linear equations.

III. NUMERICAL ANALYSIS

As Table I reveals, the moment method matrix elements are given by improper single and double integrals of very complex integrands. Evaluation of such integrals requires brute force numerical integration and as such tends to be very expensive. The accuracy and efficiency of integration can be significantly improved by a procedure presented in this section. The method is analogous to the singularity subtraction method in evaluation of singular integrals and to Kummer's transformation of slowly convergent series.

Implementation of the accelerating procedure requires the prior knowledge of the asymptotic expansions of V', V'' as $k_t \to \infty$. Table II gives the first term of the asymptotic expansions of V', V'' for a two layer grounded dielectric slab. All the relevant dimensions are indicated in Fig. 1.

A glance at Table II reveals that for the case where $z \neq z'$, the characteristic Green functions decay exponentially for large values of k_t. This means that for electromagnetically coupled patches, where the antenna and the feed are vertically separated, the integrands of $Z^{\rho x}_{m\nu,p}$, $Z^{\phi z}_{m\xi,p}$ become vanishingly small outside of some finite interval. This interval rapidly decreases as the antenna-feed separation is increased. However, in cases where the source and the observation plane coincide, i.e. $z = z'$, the integrands exhibit a much slower algebraic decay. In those situations it is most expedient to implement the accelerating procedure in order to increase the efficiency of integration.

A brief illustration of the accelerating technique now follows. Consider one of the matrix elements, namely Z^{xx}_{pq}, found in Table I. Letting V'_A denote the first term in the asymptotic expansion of V', the expression for Z^{xx}_{pq} is rewritten as follows:

$$Z^{xx}_{pq} = -\frac{1}{\pi^2}\int_0^{\infty}\int_0^{\pi/2}\left\{[V' - V'_A]\cos^2\alpha + V''\sin^2\alpha\right\} J_x^2\cos(k_t\,|\,x_p - x_q\,|\cos\alpha)k_t dk_t d\alpha +$$

$$+ \frac{(-1)}{\pi^2} \int_0^{\infty} \int_0^{\pi/2} V_A' \cos^2\alpha \, J_x^2 \cos(k_t \mid x_p - x_q \mid \cos\alpha) k_t dk_t d\alpha$$

$$= \overline{Z}_{pq}^{xx} + A_{pq}^{xx} \tag{14}$$

Note, the most dominant asymptotic term of the original integrand has been subtracted. Therefore, for large values of k_t, the modified integrand will decay considerably faster. The interval of integration in k_t required to achieve relative convergence is thereby reduced from $\sim 150\ k_o$ - $200\ k_o$ to $\sim 40\ k_o$ - $50\ k_o$, where k_o is the free space propagation constant. The integral denoted by A_{pq}^{xx} has a much simpler form and can be evaluated very efficiently. In many instances, including the case considered above, the asymptotic integral can be evaluated in closed form in terms of elementary functions.

Additional numerical analysis can be performed on the integrals listed in Table I. For example, more than one asymptotic term can be subtracted from the original integrand. However, the additional asymptotic terms give rise to singular behavior at $k_t = 0$. This difficulty can be circumvented by introducing a positive regularizing parameter u and replacing k_t by $\sqrt{u^2 + k_t^2}$ in the asymptotic expansions. This technique was used to accelerate slowly convergent infinite series in the study of infinite periodic structures [4,5].

The integrands can be further simplified by extracting the surface wave pole contributions and integrating them analytically. However, since in all practical situations the dielectrics used are lossy, the surface wave poles reside off the real axis path of integration and present no major difficulty in numerical integration.

To summarize, a method accelerating the convergence of the improper spectral integrals was outlined and illustrated. Application of this method increases the efficiency of matrix elements evaluation. Detailed analysis of all matrix elements using the accelerating technique can be found in Appendix B.

IV. EXCITATION MECHANISM AND INPUT IMPEDANCE

As is pointed out in reference [7], one of the most difficult aspects of the problem under consideration is the lack of a suitable model for the excitation mechanism. In most practical situations there exists a transition between the coaxial cable connector and the microstrip line feeding the antenna. To determine the true impedance, as would be measured by the network analyzer, the analytical model should in principle account for the coax to microstrip transition and use the coaxial line TEM mode as the primary excitation. However, this kind of rigorous analysis, though possible in prinicple, would be prohibitively complicated and expensive in computation.

References [7,8,9] advance several excitation models based upon the assumption that sufficiently far from the antenna the microstrip line supports only the quasi-TEM mode. A transmission line analogy of the feed is then introduced, wherein the antenna is seen as an impedance termination. The transmission line is excited by a lumped voltage source, as shown in Figure 3. The characteristic impedance Z_c and the propagation constant β can be calculated using the standard formulas for microstrip lines, although the presence of a dielectric overlay will modify these quantities somewhat.

In the context of the moment method solution, the lumped voltage excitation of the transmission line is equivalent to the delta gap generator. Therefore, the excitation vector $[V_i]$ has the following simple form

$$V_i = \begin{cases} 1\ , \text{ at the position of the generator } (x_i = x') \\ 0\ , \text{ otherwise} \end{cases} \tag{15}$$

One of the major advantages of this excitation model is clearly the simplicity of the voltage vector evaluation.

Solution of the matrix equation for the currents on the patch and the feed line yields the value of the current $I(x')$ at the location of the generator. A straightforward analysis of the configuration in Figure 3 shows that

$$\frac{v(x')}{I(x')} = \overleftarrow{Z}(x') + \overrightarrow{Z}(x') \tag{16}$$

As Fig. 3 indicates, the left end of the transmission line is terminated in an open circuit. This fact is a consequence of choosing basis functions which force the current to zero at the end of the microstrip line. Hence $\overleftarrow{Z}(x')$ is equal to the impedance of a section of open circuited transmission line of length $(x_{oc} - x') + \Delta l_{oc}$, where Δl_{oc} accounts for the end capacitance [10]. The antenna input impedance $\overrightarrow{Z}(x')$ can now be computed using (16) in the following manner:

$$Z_{IN} = \overrightarrow{Z}(x') = \frac{v(x')}{I(x')} - \overleftarrow{Z}(x')$$

where $v(x') = -1$, and $I(x')$, and $\overleftarrow{Z}(x')$ are known quantities.

V. THEORETICAL AND EXPERIMENTAL RESULTS

The theory outlined thus far is sufficiently general to allow, by slight adjustments of parameters, analysis of most microstrip transmission line feeding arrangements. Those include the direct edge connection, capacitive gap feed and the two-layer or proximity feed. The latter case is particularly interesting [7.11-13] because it allows the transmission line to be placed close to the ground plane, thereby reducing undesirable radiation from the feed network. At the same time the bandwidth of the microstrip antenna can be enhanced by increasing the patch to ground spacing. The results presented in this section will also show that the proximity feed has an additional advantage over other microstrip feeds in that a perfect match to a 50 Ω line can be achieved simply by selecting the proper coupling distance d (see Fig. 2).

In this section computed input impedance results for the case of the electromagnetically coupled circular patch are compared with experimental data. Shown in Figs. 4,5 are input impedance loci for a patch of radius 17.5 mm. The dielectric portions of the antenna are composed of Rexolite 2200 with relative permittivity of 2.62 and a dielectric loss tangent of approximately .001. In all cases the microstrip line exciting the antenna is 4.6 mm wide and is placed 1.6 mm above the ground plane. The impedance reference plane is in all cases located 80 mm away from the center of the patch.

The computed results in Figs. 4,5 were obtained utilizing the moment method approach outlined in Section II. Currents on the patch were approximated by entire domain basis functions, given by (9). Compared with a subsectional expansion, fewer basis functions were required to obtain numerical convergence, resulting in a more efficient solution. The results in Figs. 4,5 were computed using the basis functions in Eqs. (9a)-(9c) with the following index set: {[m,n=0; ν,ξ = 1,3], [m,n=1; ν,ξ = 0,2], [m,n=2; ν,ξ = 1,3,5], [m,n = 3; ν,ξ = 0,2,4,6]}. The currents on the microstrip transmission line were expanded in a subsectional basis set and approximately 12-15 basis functions per guide wavelength were employed in computing the data.

Figs. 4.5 display good agreement between theory and experiment. The discrepancies which do exist can be attributed to both theoretical and experimental error. The inaccuracies in computed data are possibly due to the simplifying assumptions made in the course of the formulation. For instance, the transverse current variation on the microstrip line was assumed to be uniform (see eqn. (11)), disregarding the singular edge behavior. Based on the analysis of the transverse current variation on printed dipoles performed in [5], use of a more elaborate transverse variation was deemed unnecessary for line width considered here. One of the sources of experimental error was the discontinuity encountered in the transition between the coaxial connector and the microstrip line.

VI. DISCUSSION AND CONCLUSIONS

A method for computing the input impedance of a circular patch antenna excited by a microstrip transmission line has been presented in this paper. A distinguishing feature of the present analysis is the incorporation into the formulation of the boundary conditions on the feed. This type of a rigorous treatment has several advantages, namely it yields accurate input impedance results, and is applicable to a wide variety of feeding arrangements utilizing the microstrip transmission line. The negative aspect of the rigorous treatment is the additional computational expense incurred as a result of including the feed in the formulation. Consequently, the efficiency of numerical computation is a very important consideration in the overall solution. This aspect of the problem was addressed in Section III, where a method of increasing the efficiency and accuracy of numerical computation was presented.

A difficulty of a theoretical nature encountered in the analysis was the absence of a general excitation model. In this paper the input impedance was defined and computed using an excitation model based upon the assumption that the microstrip line supports a quasi-TEM mode. This assumption seems to hold best for microstrip lines which have a relatively large width to height above ground ratios. Possible recommendations for future research include development of a more general excitation model and analysis of more sophisticated coupling structures.

LIST OF REFERENCES

[1] L.B. Felsen and N. Marcuvitz. *Radiation and Scattering of Waves*. New Jersey: Prentice Hall, 1973.

[2] W.H. Eggimann. "Higher order evaluation of electromagnetic diffraction by circular discs." *IEEE Trans. Microwave Theor. Tech.*, vol. 9, no. 5, pp. 408-418, Sept. 1961.

[3] J.J. Bowman, T.B.A. Senior, P.L.E. Uslenghi, ed., *Electromagnetic and Acoustic Scattering by Simple Shapes*. Amsterdam: North-Holland Publishing Co., 1969.

[4] W.F. Richards, "Anisotropy, Birefringence and Dispersion in Artificial Dielectrics." Ph.D. dissertation, Dept. Electrical Engineering, University of Illinois at Urbana-Champaign, 1977.

[5] S.M. Wright. "Efficient Analysis of Infinite Microstrip Arrays on Electrically Thick Substrates." Ph.D. dissertation, Dept. Electrical Engineering, University of Illinois at Urbana-Champaign, 1984.

[6] I.S. Gradshteyn, I.M. Ryzhik, *Table of Integrals, Series, and Products*. Florida: Academic Press, 1980.

[7] P.B. Katehi, N.G. Alexopoulos, "On the modeling of electromagnetically coupled microstrip antennas - the printed strip dipole," IEEE Trans. Antennas Propagat., vol. 32, no. 11, pp. 1179-1186, November 1984.

[8] R.W. Jackson, D.M Pozar, "Full wave analysis of microstrip open-end and gap discontinuities," *IEEE Trans. Microwave Theory Tech.*, vol. 33, no. 10, pp. 1036-1043, October 1985.

[9] P.B. Katehi, N.G. Alexopoulos, "Frequency dependent characteristics of microstrip discontinuities in millimeter-wave integrated circuits," *IEEE Trans. Microwave Theory Tech.*, vol. 33, no. 10, p. 1029-1036, October 1985.

[10] J.R. James, P.S. Hall, C. Wood, *Microstrip Antennas: Theory and Design*. New York: Peregrinus, 1981.

[11] H.G. Oltman, D.A. Huebner, "Electromagnetically coupled microstrip dipoles," *IEEE Trans. Antennas Propagat.*, vol. 29, pp. 151-157, Jan. 1981.

[12] R.S. Elliott, G.J. Stern, "The design of microstrip dipole arrays including mutual coupling. Part I: Theory," *IEEE Trans. Antennas Propagat.*, vol. 29, no. 5, pp. 757-760, Sept. 1981.

[13] G.J. Stern, R.S. Elliott, "The design of microstrip dipole arrays including mutual coupling. Part II: Experiment," *IEEE Trans. Antennas Propagat.*, vol. 29, no. 5, pp. 761-765, Sept. 1981.

[14] W. Gautschi, "Computational aspects of three-term recurrence relations," SIAM Review, vol. 9, no. 1, January, 1967.

APPENDIX A

The functions $U^{\pm}_{m,\nu}(k_t c/2), T^{\pm}_{n,\xi}(k_t c/2)$ are given by

$$U^{+}_{m,\nu} = \frac{\pi c m}{2k_t}\left[J_{\left|\frac{m+\nu}{2}\right|}J_{\left|\frac{m-\nu}{2}\right|} - J_{\left|\frac{m+\nu+2}{2}\right|}J_{\left|\frac{m-\nu-2}{2}\right|}\right] \tag{A1}$$

$$U^{-}_{m,\nu} = -\frac{\pi c}{2k_t}\left[\nu J_{\left|\frac{m+\nu}{2}\right|}J_{\left|\frac{m-\nu}{2}\right|} + (\nu+2)J_{\left|\frac{m+\nu+2}{2}\right|}J_{\left|\frac{m-\nu-2}{2}\right|}\right]. \tag{A2}$$

$$T^{+}_{n,\xi} = \frac{n\pi c}{k_t} J_{\left|\frac{n+\xi}{2}\right|}J_{\left|\frac{n-\xi}{2}\right|} \tag{A3}$$

$$T^{-}_{n,\xi} = \frac{\pi c^2}{2}\left[J_{\left|\frac{n+\xi+2}{2}\right|}J_{\left|\frac{n-\xi}{2}\right|} + J_{\left|\frac{n+\xi}{2}\right|}J_{\left|\frac{n-\xi+2}{2}\right|} - \frac{2n}{k_t c} J_{\left|\frac{n+\xi}{2}\right|}J_{\left|\frac{n-\xi}{2}\right|}\right] \tag{A4}$$

where in (A1-A4) "J" denotes the Bessell function of the first kind of argument $(k_t c/2)$.

TABLE I

MOMENT METHOD MATRIX ELEMENTS

1. Elements representing the interaction between the current modes on the patch:

$$Z^{\rho\rho}_{m,\omega\nu} = -\frac{\pi}{2\gamma_m}\int_0^\infty \left\{V' U^-_{m,\nu} U^-_{m,\omega} + V'' U^+_{m,\nu} U^+_{m,\omega}\delta_{0m}\right\} k_t\, dk_t \qquad \text{Notation} - \delta_{0m} = \begin{cases} 1 & m=0 \\ 0 & m\neq 0 \end{cases}$$

$$Z^{\rho\phi}_{m,\omega\xi} = -\frac{\pi}{2\gamma_m}\int_0^\infty \left\{V' T^+_{m,\xi} U^-_{m,\omega} + V'' T^-_{m,\xi} U^+_{m,\omega}\delta_{0m}\right\} k_t\, dk_t \qquad \gamma_m = 2-\delta_{0m}$$

$$Z^{\phi\rho}_{m,\xi\omega} = Z^{\rho\phi}_{m,\omega\xi}$$

$$Z^{\phi\phi}_{m,\eta\xi} = -\frac{\pi}{2\gamma_m}\int_0^\infty \left\{V' T^+_{m,\xi} T^+_{m,\eta} + V'' T^-_{m,\xi} T^-_{m,\eta}\delta_{0m}\right\} k_t\, dk_t$$

2. Elements coupling the patch modes to the transmission line:

$$Z^{\rho x}_{m\nu,p} = \frac{(-1)^{(m+1)/2}}{\pi}\int_0^\infty\int_0^{\pi/2} \left\{-V' U^-_{m,\nu}\cos m\alpha\cos\alpha + V'' U^+_{m,\nu}\sin m\alpha\sin\alpha\right\} \cdot J_x\cos(k_t x_p\cos\alpha)\cdot k_t dk_t d\alpha \quad m\text{—odd}$$

$$= \frac{(-1)^{m/2}}{\pi}\int_0^\infty\int_0^{\pi/2} \left\{-V' U^-_{m,\nu}\cos m\alpha\cos\alpha + V'' U^+_{m,\nu}\sin m\alpha\sin\alpha\right\} \cdot J_x\sin(k_t x_p\cos\alpha)\cdot k_t dk_t d\alpha \quad m\text{—even}$$

$$Z^{\phi x}_{m\xi,p} = \frac{(-1)^{(m+1)/2}}{\pi}\int_0^\infty\int_0^{\pi/2} \left\{-V' T^+_{m,\xi}\cos m\alpha\cos\alpha + V'' T^-_{m,\xi}\sin m\alpha\sin\alpha\right\} \cdot J_x\cos(k_t x_p\cos\alpha)\cdot k_t dk_t d\alpha \quad m\text{—odd}$$

$$= \frac{(-1)^{m/2}}{\pi}\int_0^\infty\int_0^{\pi/2} \left\{-V' T^+_{m,\xi}\cos m\alpha\cos\alpha + V'' T^-_{m,\xi}\sin m\alpha\sin\alpha\right\} \cdot J_x\sin(k_t x_p\cos\alpha)\cdot k_t dk_t d\alpha \quad m\text{—even}$$

3. Interaction between the current subsections on the microstrip line:

$$Z^{xx}_{pq} = -\frac{1}{\pi^2}\int_0^\infty\int_0^{\pi/2} \{V'\cos^2\alpha + V''\sin^2\alpha\} J_x^2\cos(k_t\,|\,x_p - x_q\,|\cos\alpha) k_t\, dk_t d\alpha$$

Table II

FIRST TERM IN THE ASYMPTOTIC EXPANSION of V' AND V'' As $k_t \to \infty$			
z	z'	$V'_A(z,z')$	$V''_A(z,z')$
z_1	z_1	$\dfrac{-jk_t}{\omega\epsilon_o(\epsilon_{r1}+\epsilon_{r2})}$	$\dfrac{j\omega\mu_o}{2k_t}$
z_2	z_2	$\dfrac{-jk_t}{\omega\epsilon_o(1+\epsilon_{r2})}$	$\dfrac{j\omega\mu_o}{2k_t}$
z_1	z_2	$\dfrac{-jk_t\, 2\epsilon_{r2}\, e^{-k_t t_2}}{\omega\epsilon_o(\epsilon_{r1}+\epsilon_{r2})(1+\epsilon_{r2})}$	$\dfrac{j\omega\mu_o\, e^{-k_t t_2}}{2k_t}$

APPENDIX B

EVALUATION OF THE ASYMPTOTIC INTEGRALS

Section III outlined a method for accelerating the numerical computation of Sommerfeld-type integrals. It was shown that the computational efficiency could be considerably enhanced by subtracting the slowest decaying asymptotic term of the integrand and evaluating it in closed form. The derivations of the closed form solutions for the asymptotic integrals are presented in this Appendix.

Consider the following asymptotic integral, associated with the matrix element $Z^{\rho\rho}_{m,\omega\nu}$ (Table I)

$$A^{\rho\rho}_{m,\omega\nu} = -\frac{\pi}{2\gamma_m}\int_0^\infty V_A'\, U^-_{m,\nu}\, U^-_{m,\omega}\, k_t dk_t \tag{B1}$$

where

$$U^-_{m,\nu} = \frac{c}{k_t}\int_0^1 J_m(k_t c\rho)P_\nu'(\rho)d\rho \tag{B2}$$

$$P_\nu'(\rho) = -\left|\nu T_\nu(\rho) + (\nu+2)T_{\nu+2}(\rho)\right|/\sqrt{1-\rho^2} \tag{B3}$$

$$V_A' = \frac{-jk_t}{\omega\epsilon_0(1+\epsilon_{r2})} \tag{B4}$$

"J" is a Bessel funciton of the first kind, and c is the radius of the circular patch.

Substituting (B2-B4) into (B1) and interchaning the order of integrations yields the following expression

$$A^{\rho\rho}_{m,\omega\nu} = C\int_0^1 d\tau P_\nu'(\tau)\int_0^1 d\rho P_\omega'(\rho)\left\{\int_0^\infty J_m(k_t c\rho)J_m(k_t c\tau)dk_t\right\} \tag{B5}$$

where $C = \dfrac{-jc^2}{\omega\epsilon_0(1+\epsilon_{r2})}$

The quantity in the $\{\cdots\}$ brackets is recognized as being related to the Associated Legendre function of the second kind of integer half orders [6], or more precisely

$$\int_0^\infty J_m(k_t c\rho)J_m(k_t c\tau)dk_t = \frac{1}{\pi c(\tau\rho)^{1/2}} \cdot Q_{m-\frac{1}{2}}\left|\frac{\rho^2+\tau^2}{2\rho\tau}\right| \tag{B6}$$

The function $Q_{m-1/2}$ can be numerically evaluated from its recursion relations [6] using the well-known back-recursion algorithm [14].

To enhance the clarity of the presentation it is expedient to introduce the following fundamental integral

$$I(\nu,\omega,m) = \int_0^1 d\tau \int_0^1 d\rho \frac{T_\nu(\tau)T_\omega(\rho)}{\sqrt{1-\tau^2}\sqrt{1-\rho^2}} \cdot \left\{\frac{1}{\sqrt{\rho\tau}} Q_{m-\frac{1}{2}}\left|\frac{\rho^2+\tau^2}{2\rho\tau}\right|\right\}$$

$$= \int_0^1 d\tau \int_0^\tau d\rho \frac{[T_\nu(\tau)T_\omega(\rho) + T_\nu(\rho)T_\omega(\tau)]}{\sqrt{1-\tau^2}\sqrt{1-\rho^2}} \left\{\frac{1}{\sqrt{\rho\tau}} Q_{m-\frac{1}{2}}\left|\frac{\rho^2+\tau^2}{2\rho\tau}\right|\right\} \tag{B7}$$

Utilizing (B7), the expression for $A^{\rho\rho}_{m,\omega\omega}$ can now be rewritten as follows

$$A^{\rho\rho}_{m,\omega\omega} = C_1 \Big\{\nu\omega I(\nu,\omega,m) + \nu(\omega+2)I(\nu,\omega+2,m)$$

$$+ (\nu+2)\omega T(\nu+2,\omega,m) + (\nu+2)(\omega+2)I(\nu+2,\omega+2,m)\Big\} \tag{B8}$$

where $C_1 = \dfrac{-jc}{\pi\omega\epsilon_0(1+\epsilon_{r2})}$

Related asymptotic integrals have been evaluated in an analogous manner. The resulting expressions are summarized in Table III.

Several observations concerning the evaluation of the asymptotic integrals, and more specifically the integral $I(\nu,\omega,m)$, should be made. The most important of these is the fact that $I(\nu,\omega,m)$ does not depend on any geometrical or electrical parameters of the problem. Hence it

should be computed only once for each relevant combination of integers (ν,ω,m) and then stored for subsequent recall. Furthermore, utilizing the hypergeometric function series representation for $Q_{m-1/2}$ and integrating term by term, the double integration in (B7) can be reduced to an infinite series summation.

The integral A_{pq}^{xx} of equation (14) can be evaluated in terms of elementary functions. With the aid of Table II and equation (12), A_{pq}^{xx} is rewritten as follows

$$A_{pq}^{xx} = C_x \int_0^{\omega} \int_0^{\pi/2} \cos^2\alpha \frac{\sin^4\left|\frac{\Delta k_t \cos\alpha}{2}\right|}{\left|\frac{\Delta k_t \cos\alpha}{2}\right|^4} \cdot \frac{\sin^2(k_t w \sin\alpha)}{(k_t w \sin\alpha)^2}$$

$$\cdot \cos(\Delta k_t |p-q| \cos\alpha)\, k_t^2\, dk_t d\alpha = C_x A(|p-q|) \qquad \text{(B9)}$$

where $C_x = \left|\frac{\Delta}{\pi}\right|^2 \frac{j}{\omega\epsilon_o(\epsilon_{r1}+\epsilon_{r2})}$

Formulas on pages 449-453 in reference [6] can be applied to evaluate A(|p-q|). Considerable algebra is required to obtain the final result, which is summarized in Table IV.

Note, evaluation of the asymptotic integrals associated with $Z_{m\nu,\rho}^{\rho x}$, $Z_{m\xi,\rho}^{\phi x}$ is omitted here, since it was shown in Section III that for the case of the electromagnetically coupled patch the integrands of these matrix elements decay exponentially.

TABLE III

Evaluation of Integrals $A^{\rho\rho}_{m,\omega\nu}$, $A^{\rho\phi}_{m,\omega\xi}$, $A^{\phi\phi}_{m,\eta\xi}$

$$A^{\rho\rho}_{m,\omega\nu} = C_1 \left\{ \nu\omega I(\nu,\omega,m) + \nu(\omega+2) I(\nu,\omega+2,m) + (\nu+2)\omega I(\nu+2,\omega,m) + (\nu+2)(\omega+2) I(\nu+2,\omega+2,m) \right\}$$

$$A^{\rho\phi}_{m,\omega\xi} = C_2 \left\{ \omega I(\omega,\xi,m) + (\omega+2) I(\omega+2,\xi,m) \right\}$$

$$A^{\phi\phi}_{m,\eta\xi} = C_3 I(\eta,\xi,m) + C_4 \left\{ I(\eta+1,\xi+1,m+1) + I(\eta+1,\xi-1,m+1) + I(\eta-1,\xi+1,m+1) + I(\eta-1,\xi-1,m+1) \right\}$$

Constants:

$$C_1 = \frac{c}{\pi} V'_{A0} \; ; \; C_2 = \frac{-2mc}{\pi} V'_{A0} \; ; \; C_3 = \frac{4m^2 c}{\pi} V'_{A0} \; ; \; C_4 = \frac{c^3}{\pi} V''_{A0}$$

$$V'_{A0} = \frac{-j}{\omega\epsilon_0(1+\epsilon_{r2})} \; ; \; V''_{A0} = \frac{j\omega\mu_0}{2}$$

Notes:

1) $I(\nu,\omega,m) = I(\omega,\nu,m)$; $I(\nu,-\omega,m) = I(\nu,\omega,m)$

2) The second term in $A^{\phi\phi}_{m,\eta\xi}$ results from subtraction of V''_A from the original integrand

TABLE IV

Evaluation of $A_{pq}^{xx} = C_x A(|p-q|)$

$$A(0) = \frac{\pi}{8}(2K_3-K_4)\int_{\alpha=l_0}^{l_1} + \frac{\pi}{24}(-4K_1+12K_2-6K_3+K_4)\int_{\alpha=l_1}^{l_2} + \frac{\pi}{6}K_1\int_{\alpha=l_2}^{l_\infty}$$

$$A(1) = \frac{\pi}{24}(2K_4-3K_3)\int_{\alpha=l_0}^{l_1} + \frac{\pi}{48}(7K_1-21K_2+15K_3-3K_4)\int_{\alpha=l_1}^{l_2} +$$

$$+ \frac{\pi}{48}(-25K_1+27K_2-9K_3+K_4)\int_{\alpha=l_2}^{l_3} + \frac{\pi}{24}K_1\int_{\alpha=l_3}^{l_\infty}$$

$$A(n)\big|_{n\geq 2} = \frac{\pi}{48}[(n-2)^3K_1-3(n-2)^2K_2+3(n-2)K_3-K_4]\int_{\alpha=l_{n-2}}^{l_{n-1}} -$$

$$- \frac{\pi}{48}[(3n^3-6n^2+4)K_1-(9n^2-12n)K_2+(9n-6)K_3-3K_4]\int_{\alpha=l_{n-1}}^{l_n} -$$

$$- \frac{\pi}{48}[(-3n^3-6n^2+4)K_1+(9n^2+12n)K_2-(9n+6)K_3+3K_4]\int_{\alpha=l_n}^{l_{n+1}} -$$

$$- \frac{\pi}{48}[(n+2)^3K_1-3(n+2)^2K_2+3(n+2)K_3-K_4]\int_{\alpha=l_{n+1}}^{l_{n+2}}$$

Definitions

1. $K_1 = -\frac{\Delta}{2w^2}\frac{1}{\sin\alpha}$; $K_2 = \frac{1}{w}\ln\left|\tan\frac{\alpha}{2}\right|$;

$K_3 = \frac{2}{\Delta}\ln\left|\tan\left|\frac{\pi}{4}+\frac{\alpha}{2}\right|\right|$; $K_4 = \frac{4w}{\Delta^2}\frac{1}{\cos\alpha}$

2. $l_n = \arctan\left|\frac{n\Delta}{2w}\right|$; $l_0 = 0$; $l_\infty = \frac{\pi}{2}$

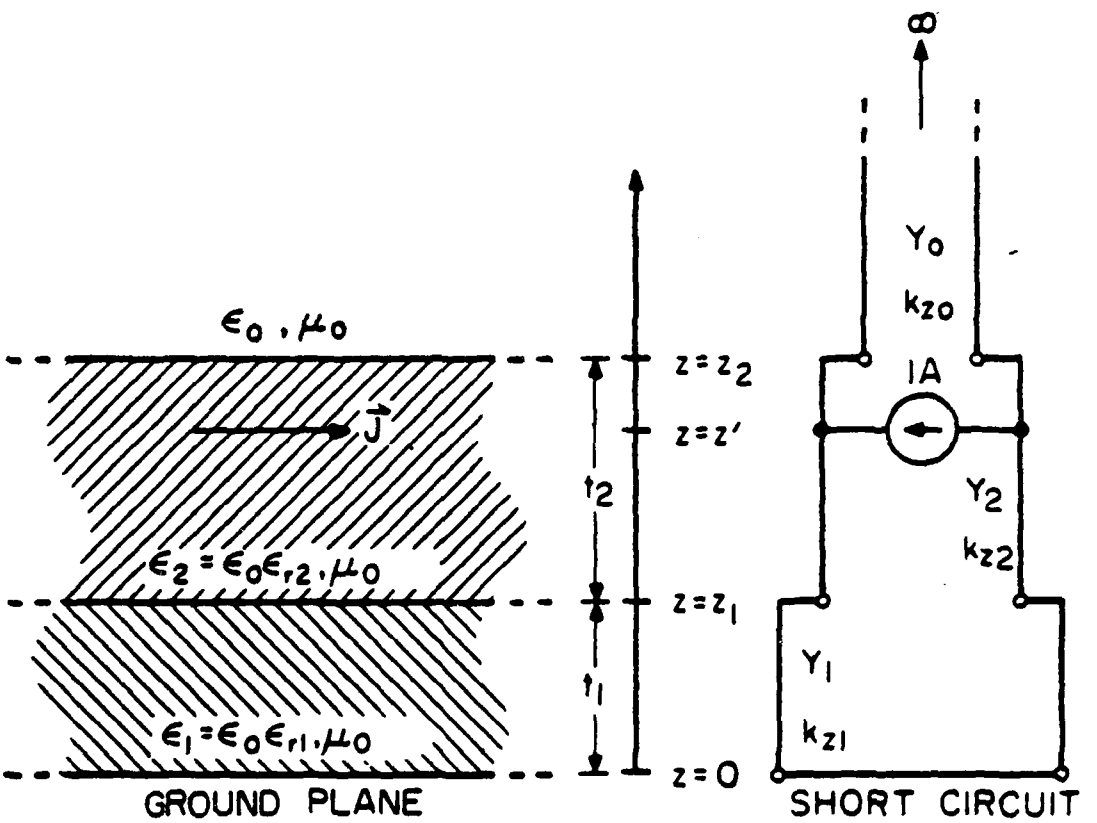

Figure 1. Two-layer grounded dielectric slab and its equivalent circuit representation.

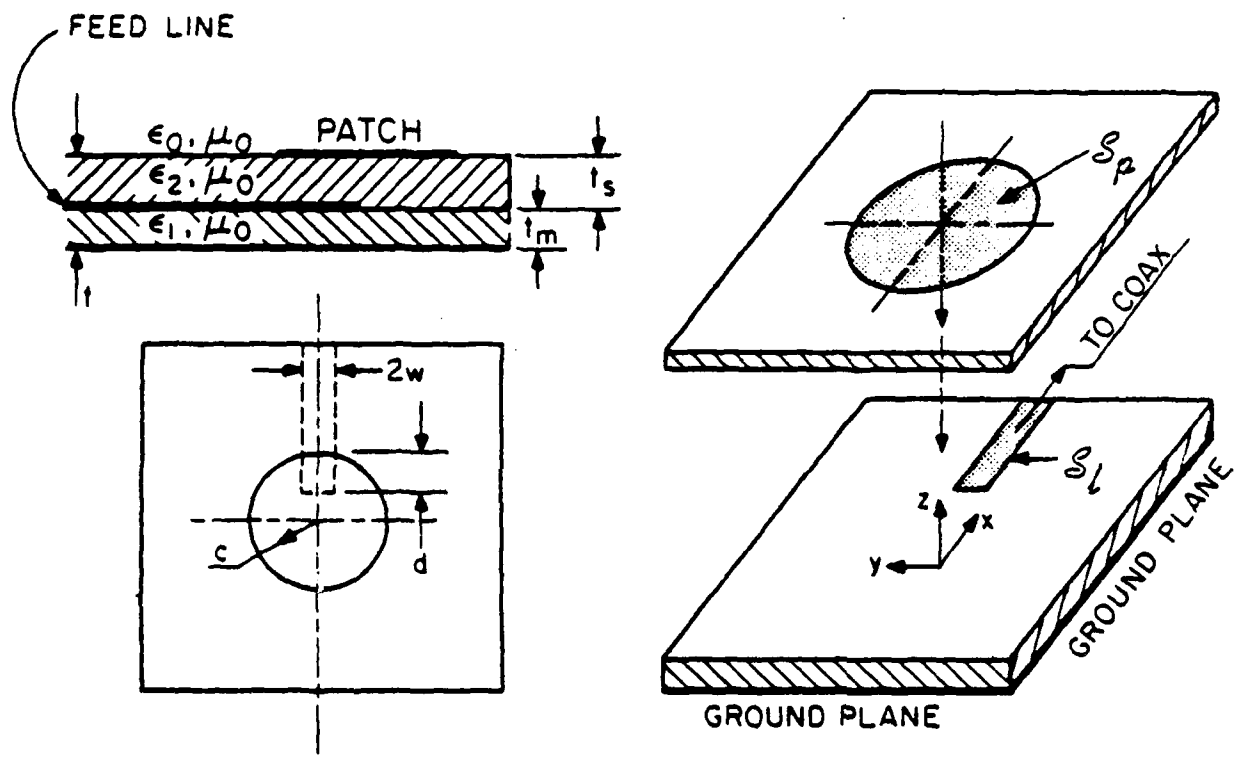

Figure 2. Circular patch antenna excited by a microstrip transmission line.

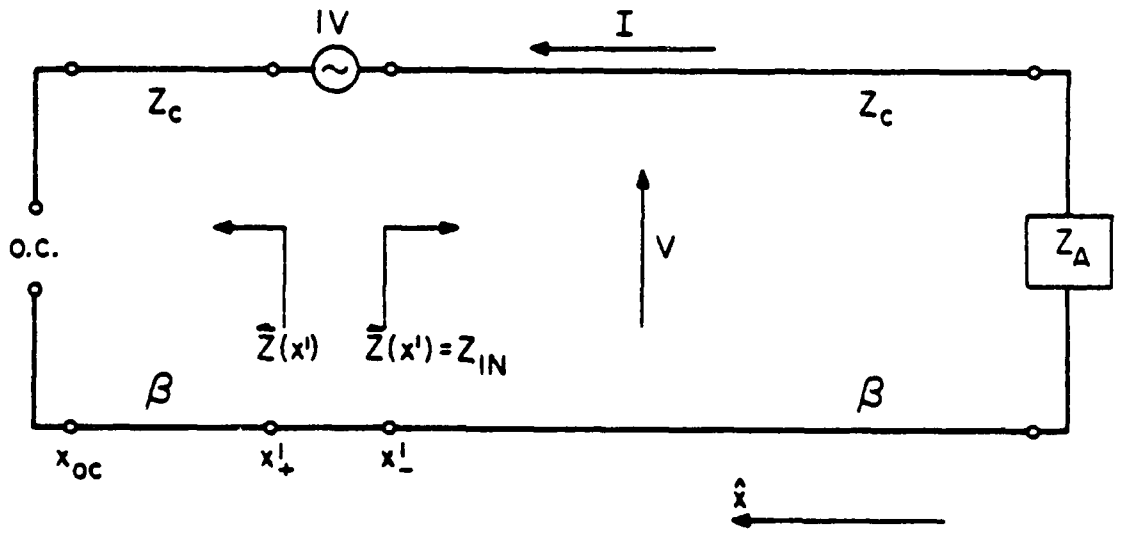

Figure 3. Transmission line model of the electromagnetically coupled circular patch antenna, showing the voltage source and input impedance definition.

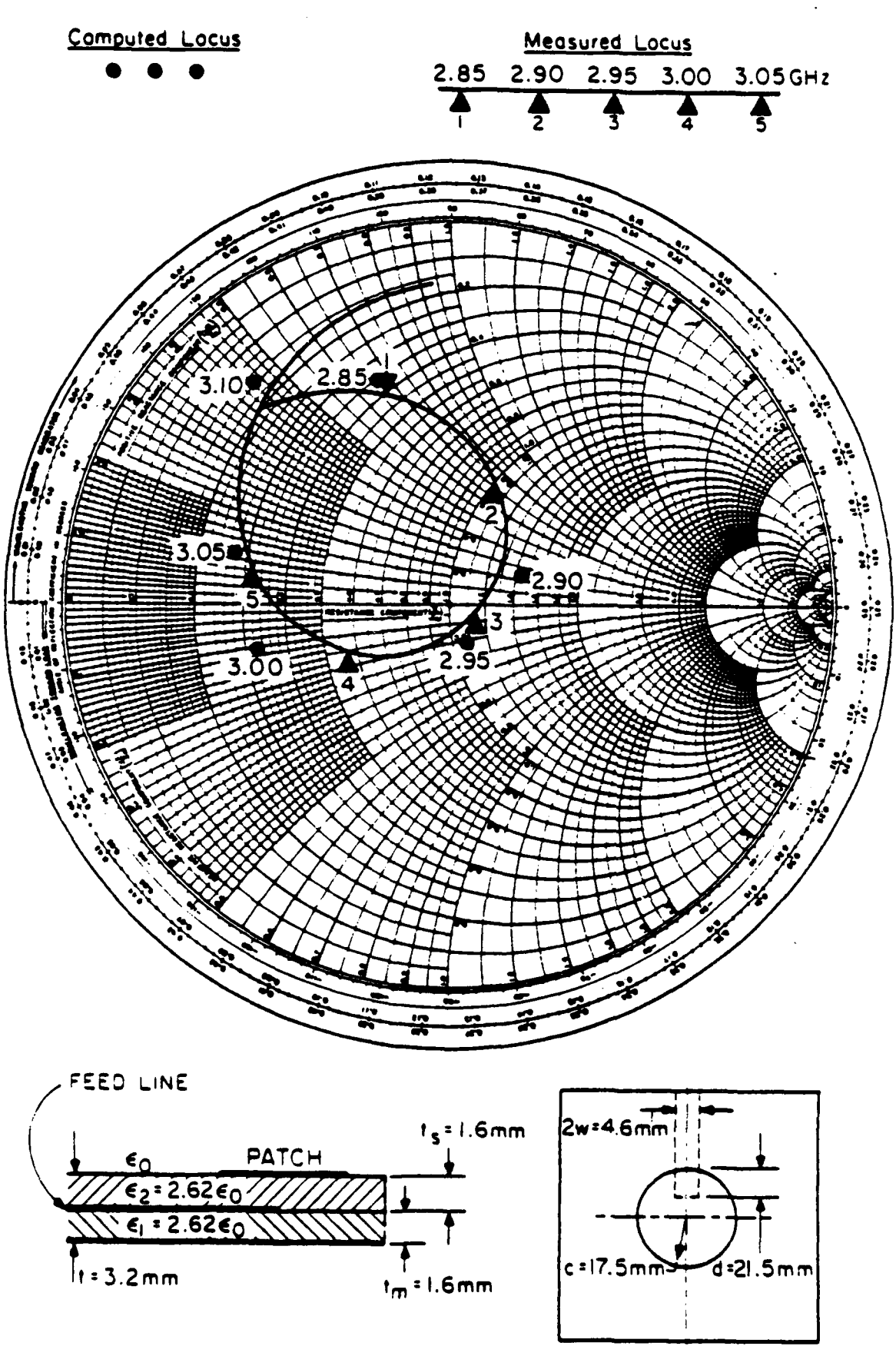

Figure 4(a-d). Input impedance of electromagnetically coupled circular patch.

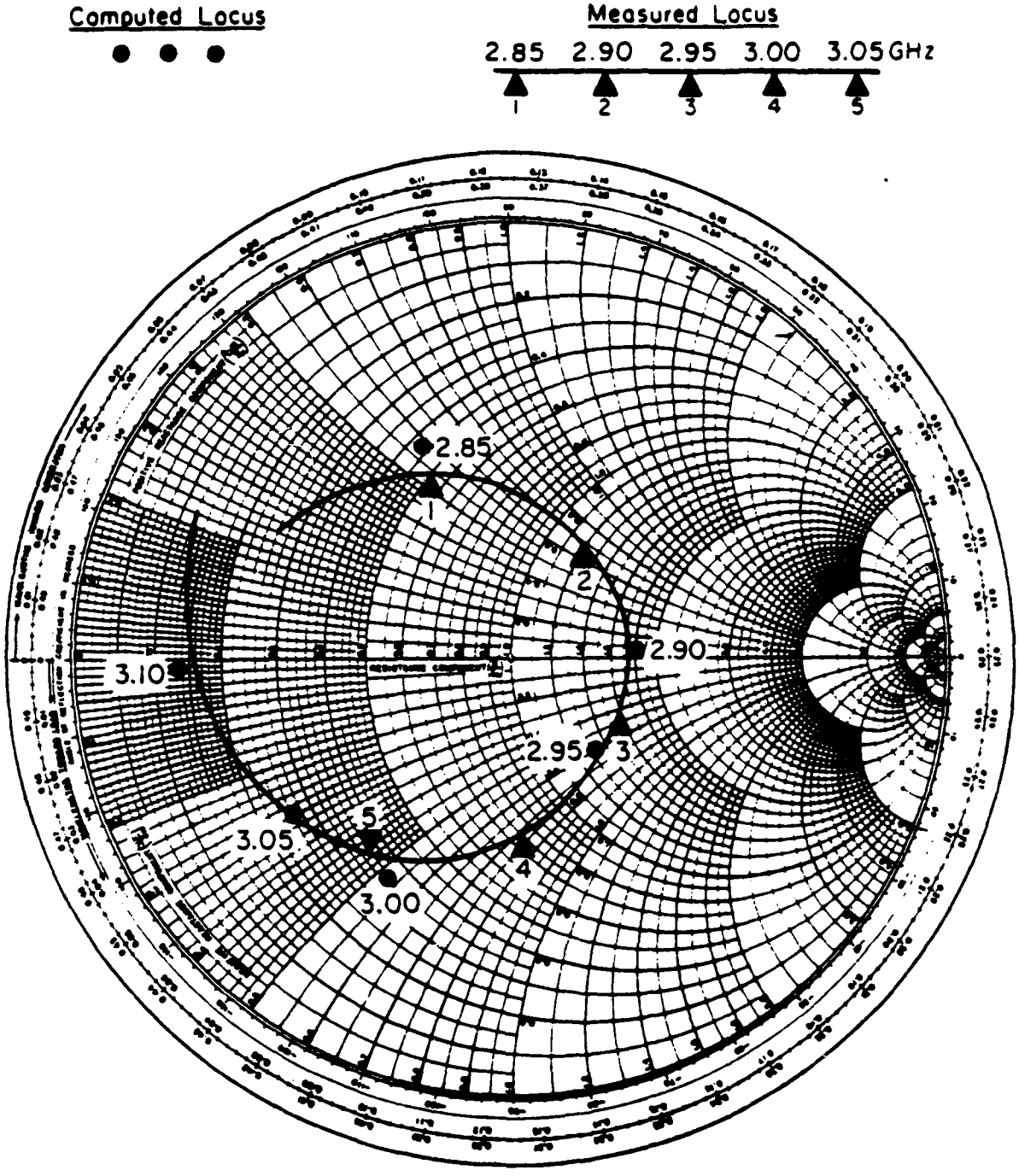
Computed Locus
Measured Locus
2.85 2.90 2.95 3.00 3.05 GHz
1 2 3 4 5
2.85
2.90
3.10
2.95
3.05
3.00

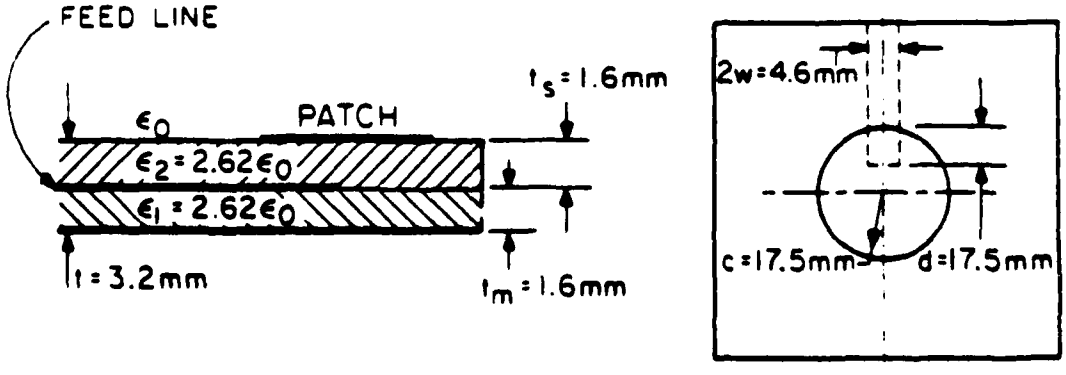
FEED LINE
t_s = 1.6mm
ϵ_0
PATCH
$\epsilon_2 = 2.62\epsilon_0$
$\epsilon_1 = 2.62\epsilon_0$
t = 3.2mm
t_m = 1.6mm
2w = 4.6mm
c = 17.5mm
d = 17.5mm

Figure 4(b)

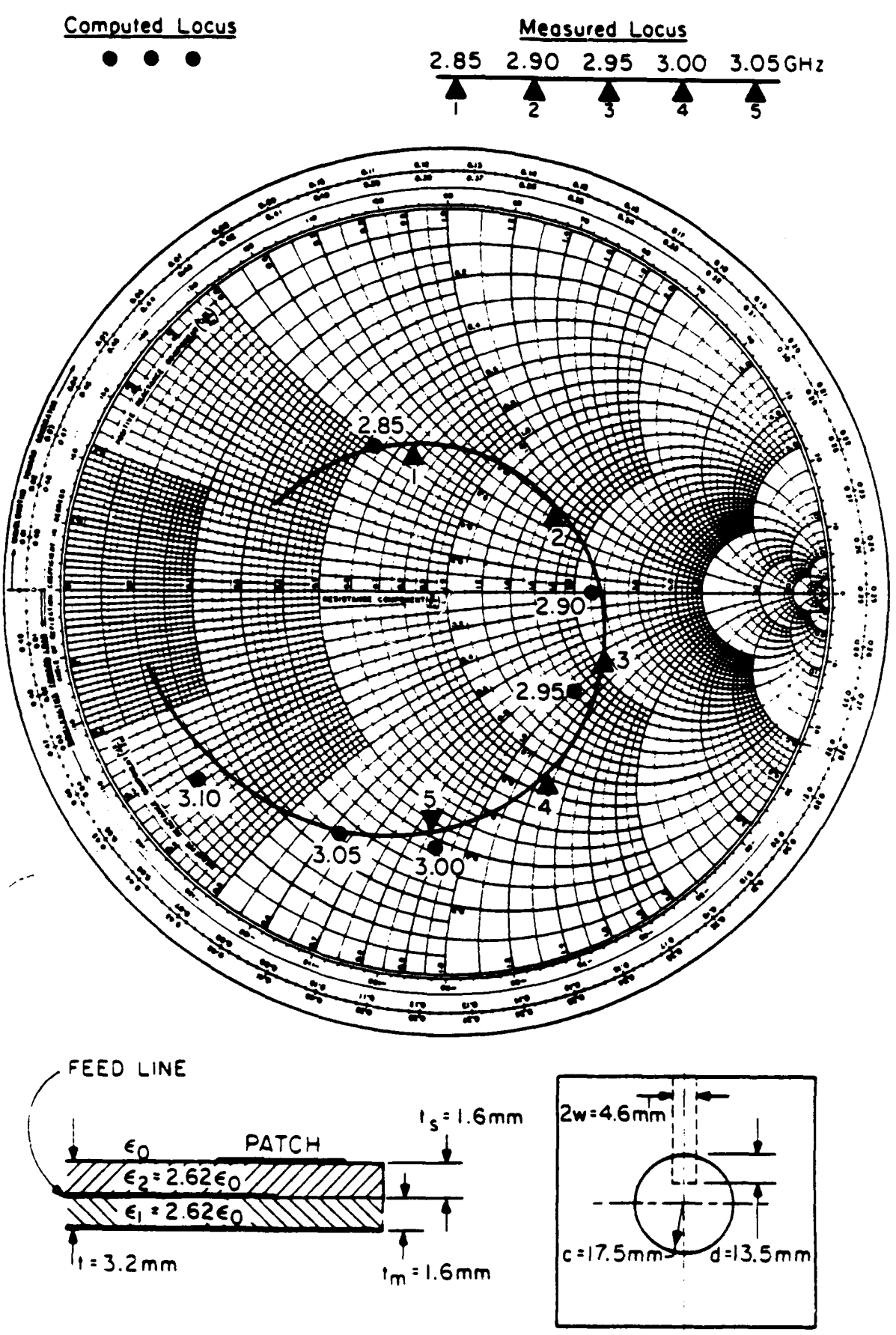
Computed Locus
Measured Locus
2.85 2.90 2.95 3.00 3.05 GHz
1 2 3 4 5
2.85
2.90
2.95
3.00
3.05
3.10
FEED LINE
ϵ_0
PATCH
$\epsilon_2 = 2.62\epsilon_0$
$\epsilon_1 = 2.62\epsilon_0$
$t_s = 1.6$mm
$t = 3.2$mm
$t_m = 1.6$mm
2w=4.6mm
c=17.5mm
d=13.5mm

Figure 4(c)

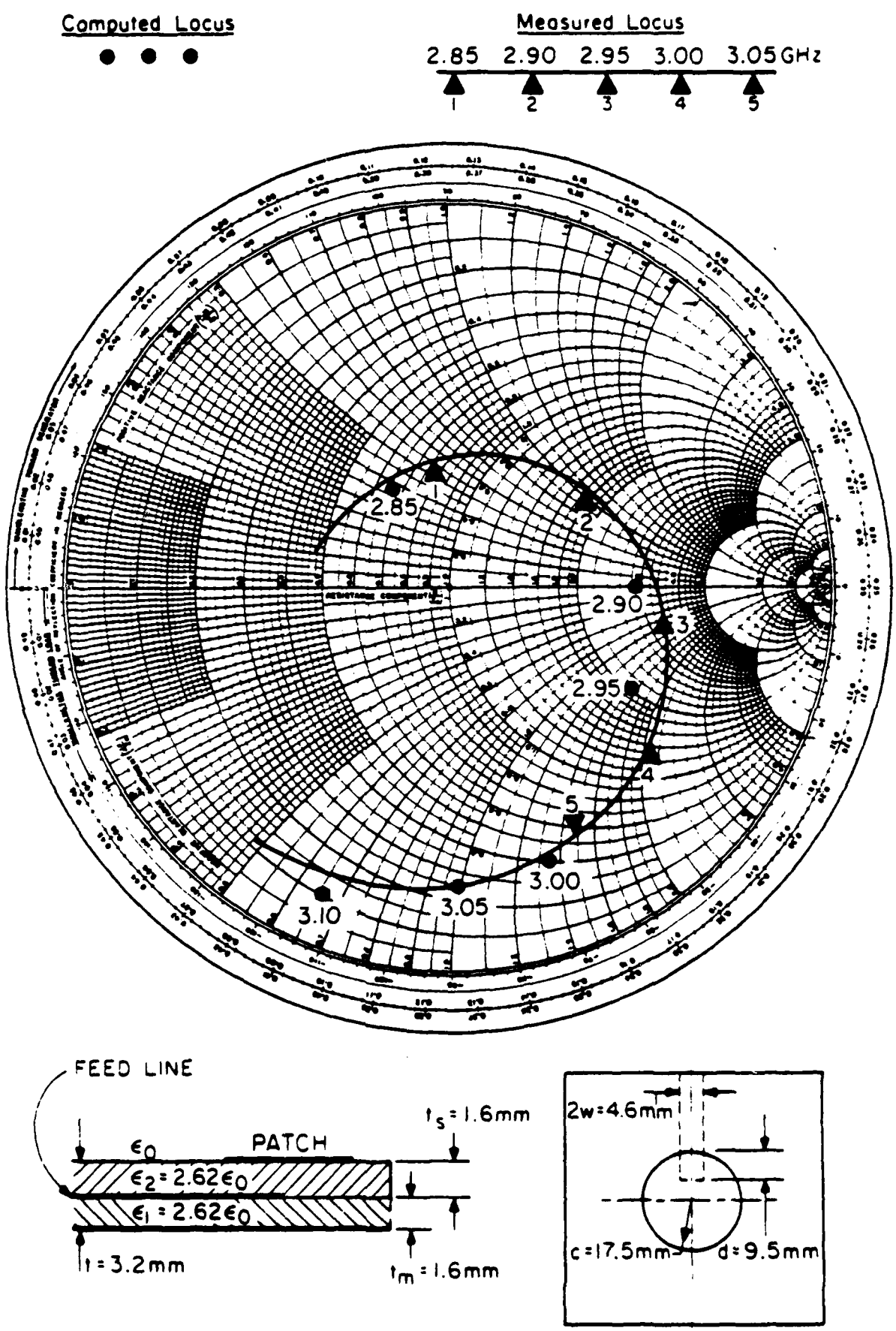
Computed Locus
Measured Locus
2.85 2.90 2.95 3.00 3.05 GHz
1 2 3 4 5
2.85
2.90
2.95
3.00
3.05
3.10
FEED LINE
t_s = 1.6mm
ϵ_0
PATCH
$\epsilon_2 = 2.62\epsilon_0$
$\epsilon_1 = 2.62\epsilon_0$
t = 3.2mm
t_m = 1.6mm
2w = 4.6mm
c = 17.5mm
d = 9.5mm

Figure 4(d)

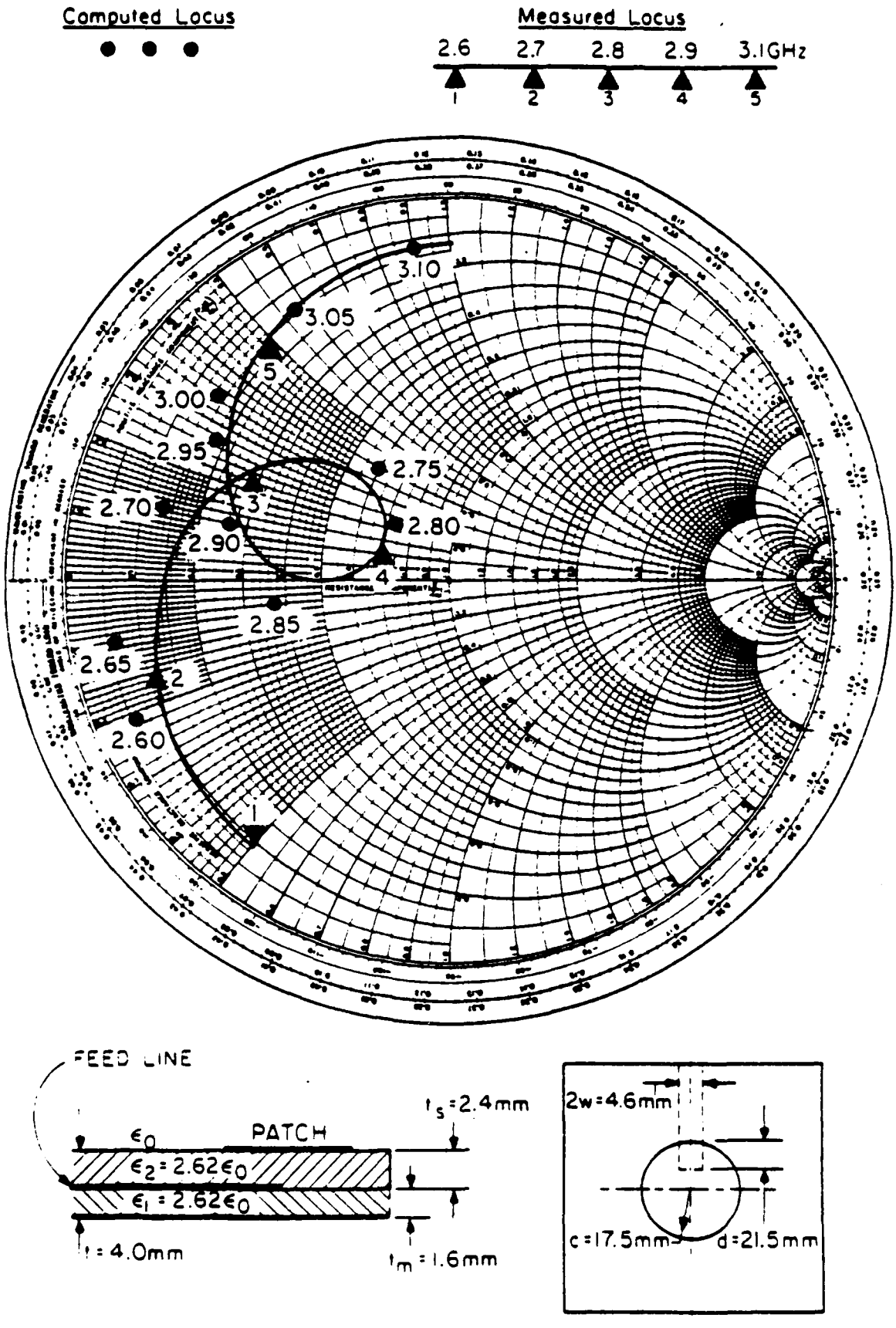

Figure 5(a-c). Input impedance of electromagnetically coupled circular patch.

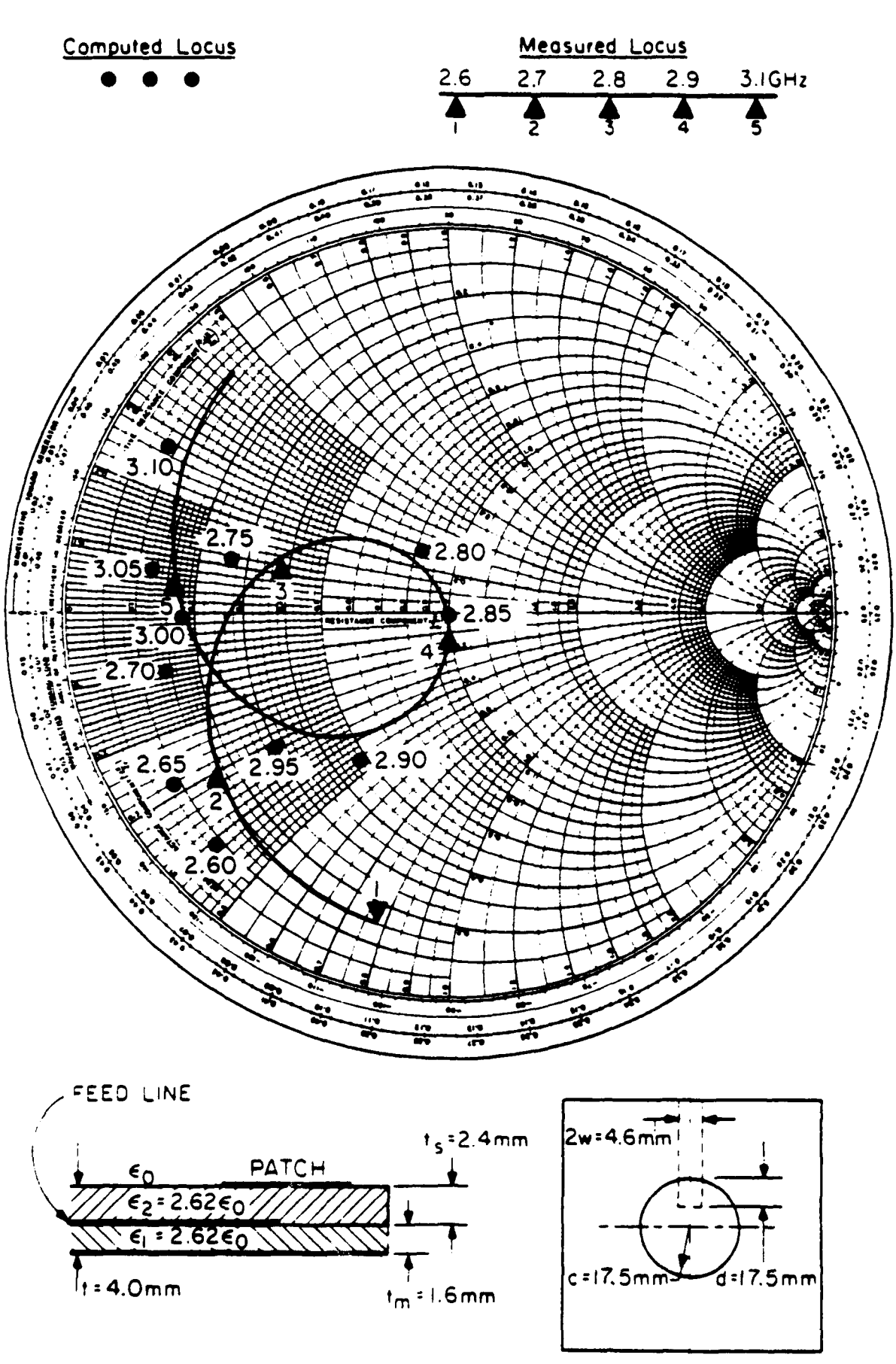
Computed Locus
Measured Locus
2.6
2.7
2.8
2.9
3.1GHz
1
2
3
4
5
3.10
2.75
2.80
3.05
3
2.85
5
3.00
4
2.70
2.65
2.95
2.90
2
2.60
1
FEED LINE
t_s = 2.4mm
ϵ_0
PATCH
$\epsilon_2 = 2.62\epsilon_0$
$\epsilon_1 = 2.62\epsilon_0$
t = 4.0mm
t_m = 1.6mm
2w = 4.6mm
c = 17.5mm
d = 17.5mm

Figure 5(b)

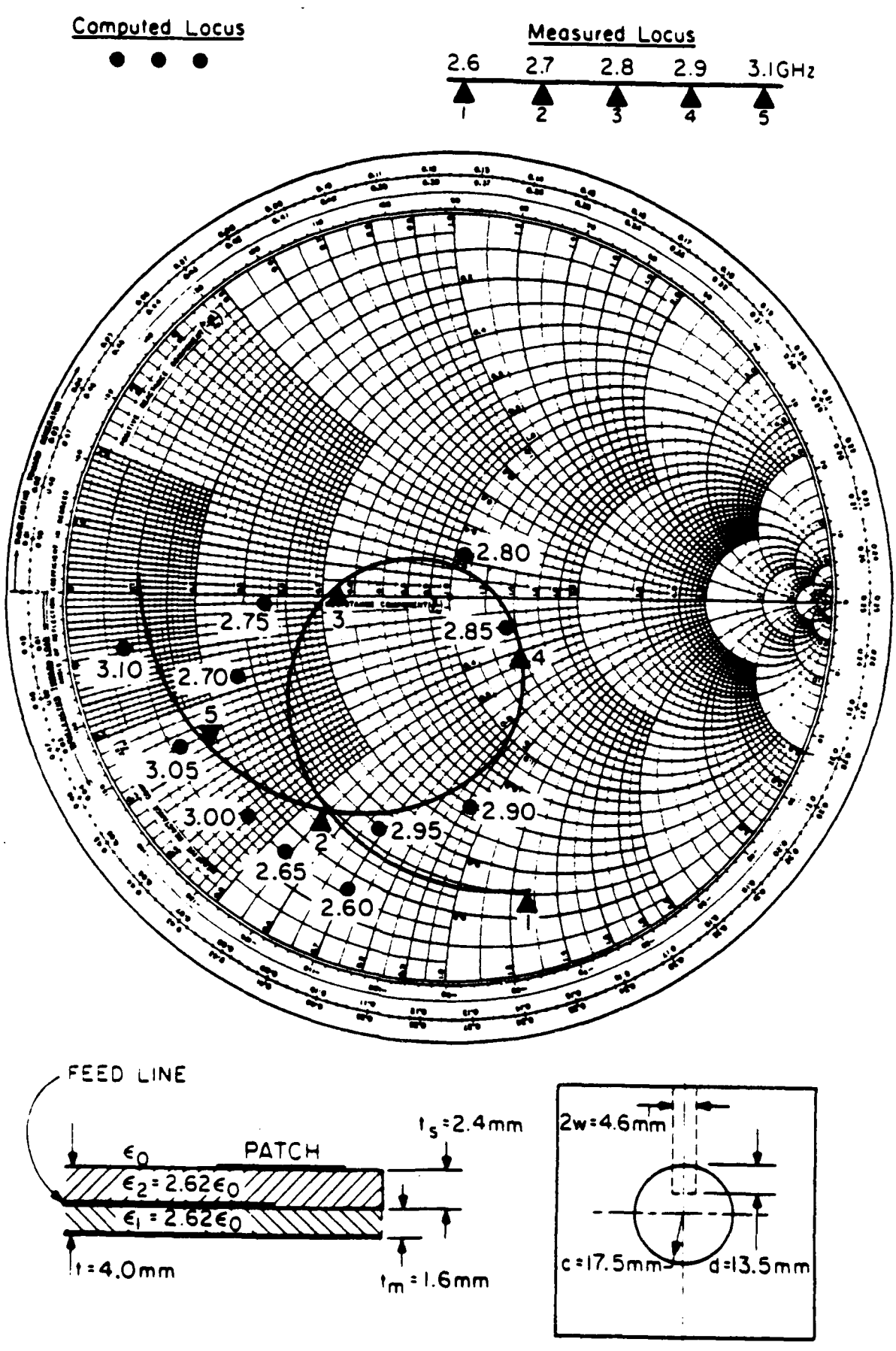
Computed Locus
Measured Locus
2.6
2.7
2.8
2.9
3.1GHz
1
2
3
4
5
2.80
2.75
2.85
3.10
2.70
3.05
3.00
2.95
2.90
2.65
2.60
FEED LINE
t_s = 2.4mm
ϵ_0
PATCH
$\epsilon_2 = 2.62\epsilon_0$
$\epsilon_1 = 2.62\epsilon_0$
t = 4.0mm
t_m = 1.6mm
2w = 4.6mm
c = 17.5mm
d = 13.5mm

Figure 5(c)

MISSION
of
Rome Air Development Center

RADC plans and executes research, development, test and selected acquisition programs in support of Command, Control Communications and Intelligence (C^3I) activities. Technical and engineering support within areas of technical competence is provided to ESD Program Offices (POs) and other ESD elements. The principal technical mission areas are communications, electromagnetic guidance and control, surveillance of ground and aerospace objects, intelligence data collection and handling, information system technology, solid state sciences, electromagnetics and electronic reliability, maintainability and compatibility.

Printed by
United States Air Force
Hanscom AFB, Mass. 01731